Am J Cancer Res 2023;13(10):4903-4917
www.ajcr.us /ISSN:2156-6976/ajcr0152492

Original Article

Preclinical trial of targeting the Hic-5-mediated pathway to prevent the progression of hepatocellular carcinoma

Wen-Sheng Wu[1,2], Chuan-Chu Cheng[1], Yi-Hsuan Lee[1], Jia-Ling Wei[1], Rui-Fang Chen[1], Chen-Fang Lin[1,2], Ren-In You[2], Yen-Chang Chen[3,4], Hsiu-Ming Shih[5], Chi-Tan Hu[6], Hsin-Hou Chang[7], Ming-Che Lee[8,9], Yen-Cheng Chen[1,10]

[1]Division of General Surgery, Department of Surgery, Hualien Tzu Chi Hospital, Buddhist Tzu Chi Medical Foundation, Hualien 97004, Taiwan; [2]Department of Laboratory Medicine and Biotechnology, College of Medicine, Tzu Chi University, Hualien 97004, Taiwan; [3]Department of Anatomical Pathology, Hualien Tzu Chi Hospital, Buddhist Tzu Chi Medical Foundation, Hualien 97004, Taiwan; [4]Department of Pathology, School of Medicine, Tzu Chi University, Hualien 97004, Taiwan; [5]Institute of Biomedical Sciences, Academia Sinica, Taipei 11529, Taiwan; [6]Division of Gastroenterology, Department of Medicine, Research Centre for Hepatology, Hualien Tzu Chi Hospital, Buddhist Tzu Chi Medical Foundation, Hualien 97004, Taiwan; [7]Department of Molecular Biology and Human Genetics, Tzu Chi University, Hualien 97004, Taiwan; [8]Division of General Surgery, Department of Surgery, Wan Fang Hospital, Taipei Medical University, Taipei 110, Taiwan; [9]Department of Surgery, School of Medicine, College of Medicine, Taipei Medical University, Taipei 110, Taiwan; [10]School of Medicine, Tzu Chi University, Hualien 97004, Taiwan

Received July 28, 2023; Accepted September 23, 2023; Epub October 15, 2023; Published October 30, 2023

Abstract: The poor prognosis of hepatocellular carcinoma (HCC) was ascribed to metastasis. Targeted therapy aiming at the molecules along the metastatic pathway is a promising therapeutic strategy. Among them, hydrogen peroxide inducible clone-5 (Hic-5) is highlighted. Hic-5, discovered as a reactive oxygen species (ROS)-inducible gene, was identified to be an adaptor protein in focal adhesion and a critical signaling mediator upregulated in various cancers including HCC. Moreover, Hic-5 may regulate epithelial-mesenchymal transition (EMT) transcription factor Snail and its downstream mesenchymal genes including fibronectin and matrix metalloproteinase-9 required for migration and invasion of HCC. However, the comprehensive Hic-5-mediated pathway was not established and whether Hic-5 can be a target for preventing HCC progression has not been validated *in vivo*. Using whole-transcriptome mRNA sequencing, we found reactive oxygen species modulator (ROMO) and ZNF395 were upregulated by Hic-5 in a patient-derived HCC cell line, HCC372. Whereas ROMO was involved in Hic-5-mediated ROS signaling, ZNF395 locates downstream of Snail for mesenchymal genes expression required for cell migration. Also, ZNF395 but not ROMO was upregulated by Hic-5 for migration in another patient-derived HCC cell line, HCC374. Further, by *in vivo* knock down of Hic-5 using the Stable Nucleic Acids Lipid nanoparticles (SNALP)-carried Hic-5 siRNA, progression of HCC372 and HCC374 in SCID mice was prevented, coupled with the decrease of the downstream mesenchymal genes. Our study provides the preclinical evidence that targeting Hic-5 is potentially able to prevent the progression of HCCs with Hic-5 overexpression.

Keywords: Hic-5, reactive oxygen species modulator, ZNF395, metastasis, stable nucleic acids lipid nanoparticles

Introduction

Hepatocellular carcinoma (HCC) is one of the most common types of cancers, with an increasing incidence globally [1]. Metastasis is responsible for high rates of disease recurrence, which lead to poor prognosis of HCC [1-3]. Tumor metastasis is initiated by epithelial-mesenchymal transition (EMT), migration and invasion, followed by intravasation, extravasation, and colonization on metastatic loci [4, 5]. Numerous growth factors and cytokines, such as epidermal growth factor (EGF) and hepatocyte growth factor (HGF), are capable of triggering metastatic changes in primary tumors [6, 7]. Target therapy aiming at the critical molecules involved in the metastatic signaling pathway is promising. Among these molecules,

hydrogen peroxide inducible clone-5 (Hic-5) has attracted considerable research attention.

Hic-5 was discovered as a transforming growth factor β (TGFβ)- and reactive oxygen species (ROS)-inducible gene [8]. It is the molecule most homologous to paxillin, one of the essential signaling adaptor proteins in focal adhesion [9, 10]. Recently, Hic-5 is found to be a critical signaling mediator frequently upregulated in various types of cancers, including breast cancer [11], colorectal cancer [12], and HCC [13, 14]. Importantly, Hic-5 expression can be stimulated by numerous metastatic factors, including HGF [11], interleukin-1β (IL-1β), stromal cell-derived factor-1 (SDF2) [12], TGFβ1 [15] and the tumor promoter 12-O-tetradecanoylphorbol-13-acetate (TPA) [16], as well as engagement with the extracellular matrix [17]. Moreover, Hic-5 can regulate the expression of genes involved in EMT through a variety of regulatory effects on signaling and transcription [18]. Our previous study revealed that Hic-5 was overexpressed in a significant proportion of HCCs, most of which are potentially metastatic [13]. Moreover, there is a cross-talk between Hic-5 and ROS-c-Jun N-terminal kinase (ROS-JNK) signaling for the induction of mesenchymal genes, including matrix metalloproteinase-9 (MMP9), Snail (SNA), zinc finger E-box binding homeobox-1 (Zeb-1), and fibronectin (FN) in HCC cell lines [13, 14]. However, the ROS signaling and transcriptional mechanisms mediated by Hic-5 have not been fully elucidated. On the other hand, although silencing of Hic-5 *in vitro* may suppress the migration and invasion of pancreatic tumor [19] and HCC [13, 14], the feasibility of Hic-5 and its downstream genes as targets for preventing HCC progression has not been investigated *in vivo*. In addition, HCC represents a group of heterogeneous tumors with diverse molecular alterations [20], implying that the signal pathway responsible for triggering HCC progression may differ between patients. Thus, it is essential to identify HCC tumors with high Hic-5 expression; this approach would facilitate the selection of patients with HCC who are suitable for Hic-5-based targeted therapy.

In this study, surgically resected HCC tissues were used to evaluate the potential correlation of Hic-5 overexpression with HCC metastasis, as well as to establish patient-derived HCC cell lines. In one of these cell lines, we identified two of the Hic-5-upregulated genes involved in HCC progression, namely reactive oxygen species modulator (ROMO) and zinc finger protein 395 (ZNF395). Moreover, by *in vivo* knockdown of Hic-5 using Stable Nucleic Acid-Lipid nanoparticles (SNALP) that carried Hic-5 siRNA, targeting Hic-5 for the prevention of HCC progression was established in SCID mice.

Material and methods

Collection of HCC tissues

Tissues were collected during surgery for the resection of HCCs at Buddhist Tzu Chi General Hospital (Hualien, Taiwan). Patient's consent was provided prior to performing this collection. This was approved by the Research Ethics Committee of Buddhist Tzu Chi General Hospital (approval number: IRB109-148-A). The tissues collected were snap frozen at -80°C before being processed for western blotting or immunohistochemistry (IHC) analysis.

Establishing patient-derived primary HCC cell lines

Patient-derived HCC cell lines were established as models to investigate HCC progression as previously reported [13]. Briefly, fresh HCC tissues were cut into small pieces, pretreated with collagenase, and cultivated on the mitomycin C-treated NIH3T3 feeder layer for 4-6 passages; tumor cell lines were then selected after 20-30 passages. The cell lines obtained by this method, namely HCC372 and HCC374, were authenticated by human short-tandem repeat analysis (Supplementary Figure 1).

Antibodies and chemicals

Antibodies against various signal molecules, including Hic-5 (GTX108510), Snail (GTX125-918, sc-10433), metalloproteinase-9 (GTX-100458, sc-393859), zinc finger E-box binding homeobox-1 (sc-515797), fibronectin (sc-8422), reactive oxygen species modulator (ab236409) and ZNF395 (sc-515519) were purchased from Santa Cruz (Dallas, TX, USA) and GeneTex (Irvine, CA, USA). Dithiothreitol (DTT) was purchased from Sigma (St. Louis, MO, USA).

RNA interference

The expression of indicated gene was transiently knocked down by treatment with siRNAs (Thermo Scientific, Dharmacon, Lafayette, CO,

USA) for 48 h. Depletions of the indicated molecules were validated by western blotting and reverse transcription-polymerase chain reaction (RT-PCR).

RT-PCR and western blotting

RT-PCR and western blotting were performed as previously described [13, 14]. Band intensities on the blots were quantified using the Image J. software (version 1.50 i; National Institutes of Health, Bethesda, MD, USA, RRID:SCR_003070). The primer sequences used in RT-PCR are shown in Supplementary Table 1.

Proliferation assay

Cell proliferation assay was performed using 3-[4,5-dimethylthiazol-2-yl]-2,5-diphenyl tetrazolium bromide (MTT). The method is based on the reduction of MTT to purple formazan crystals by metabolically active cells.

Transwell migration assay

Cells were seeded in a 24-well trans-well migration insert (Nalge Nunc International, Rochester, NY, USA) for 24 h. After appropriate treatments, cells on both the topside and underside of the insert membrane were stained with 0.3% crystal violet. The cells on the topside of the insert membrane were then rubbed with a cotton swab. The migrated cells remaining on the underside were imaged using phase contrast microscopy with 40× magnification. Quantitation of the migrated cells was performed by measuring the intensity of crystal violet staining, using Image J. software (version 1.50 i; National Institutes of Health, RRID: SCR_003070).

Invasion assay

Cells were seeded in a 24-well tran-swell migration insert coated with Matri-gel (Corning, Bedford, MA, USA) for 24 h. After appropriate treatments, cells that had invaded to the underside of the insert membrane were detected as for the migration assay described above.

Immunohistochemistry (IHC) analysis

IHC analysis was performed by the EnVision+ Dual Link System-HRP (DAKO, Carpinteria, CA, USA), a two-step staining technique using an HRP labelled polymer conjugated with secondary antibodies. Briefly, the tissue section was incubated with Dual Endogenous Enzyme Block to remove any endogenous peroxidase activity. Subsequently, the sample was incubated with primary antibody for 30 min, followed by the 2nd Ab-HRP labeled polymer for 30 min. Staining was completed by a 5-10 min incubation with diaminobenzidine (DAB) substrate chromogen, which resulted in a brown-colored precipitate at the antigen site.

Whole-transcriptome mRNA sequencing

Whole-transcriptome mRNA sequencing was used to compare the gene expression profiles between HCC cells transfected with Hic-5 siRNA and non-targeting (N-T) siRNA. Human One Array Plus Gene Expression Profiling by Phalanx Biotech Group (Hsinchu, Taiwan) was used in this analysis.

ROS generation assay

ROS generation was monitored by oxidation of permeable dye 2',7'-dichlorodihydrofluorescein diacetate (DCF-DA). After entering the cells, DCF-DA is hydrolyzed into DCF and oxidized by ROS into a fluorescent product. This product was detected at 488 nm wavelength using a Gallios flow cytometer (Beckman Coulter Taiwan Inc., Taiwan Branch, Taipei, Taiwan).

Preparation of nanoparticles carrying Hic-5 siRNA

SNALP-Hic-5si was prepared as previously reported [21]. Briefly, D-Lin-DMA and PEG-C-DMA were formulated with DSPC, cholesterol, and Hic-5 siRNA, using a 25:1 lipid/siRNA ratio and a 48/40/10/2 molar ratio of cholesterol/D-Lin-DMA/DSPC/PEG-C-DMA. In the animal experiments, SNALP carried Hic-5 siRNA (50 mg siRNA/kg mouse) was administered by tail-vein injection twice weekly for 3 weeks.

Xenograft establishment and targeted therapy in vivo

Patient-derived HCC cells (400×10^4) were subcutaneously inoculated into the flanks of severe combined immunodeficiency (SCID) mice. The tumor tissues were cut into pieces of equal size (diameter: 0.2 cm) and implanted

into the middle lobe of livers to develop HCC. One week after xenograft implantation, the mice were treated with SNALP-Hic-5si *via* tail-vein injection twice weekly. At 1-2 months after administration, we examined whether the development of patient-derived HCC in mice treated with SNALP-Hic-5si was suppressed compared with that in mice treated with SNALP-empty (i.e., without incorporation of Hic-5 siRNA). The animal experiments conducted in the present study were approved by the Institutional Animal Care and Use Committee at Tzu Chi University (approval number: 109-091). Moreover, regulations relevant to the care and use of laboratory animals were followed.

Statistical analysis

Pearson's correlation analysis was performed to assess the association of elevated Hic-5 expression with metastatic HCCs. Analysis of Variance was conducted to evaluate the differences between samples in western blotting, IHC, cell migration and invasion analyses, as well as differences in size between the tumors that developed on the livers of mice under the indicated experimental conditions. Quantitative data were expressed as the mean ± coefficient of variation.

Data availability

The data generated in this study are available within the article and its Supplementary Data.

Results

Evaluation of Hic-5 in HCCs and establishment of patient-derived HCCs with overexpression of Hic-5

A total of 50 HCCs were collected to examine the altered expression of Hic-5 in HCCs. Western blotting revealed that Hic-5 expression was significantly increased in approximately 25% of HCC tissues. Consistent with the previous finding [13], 80% of the HCC tumors with increased levels of Hic-5 have considerable metastatic potential (Pearson's correlation coefficients: $R = 0.85$; $P < 0.05$; $n = 12$) according to the clinicopathological characteristics, including the presence of tumor cells in the lymph-vascular system and the great extent of tumor invasion in the lymph nodes (Supplementary Table 2). Representative western blotting data of 10 metastatic HCCs (SD12, 13, 28, 55, 77, 78, 128; TS305, 328, 330) are demonstrated in **Figure 1A**, revealing a 2-4-fold increase in Hic-5 expression in HCC tumors compared with their normal counterparts. IHC analysis of these HCCs confirmed the significant elevation of Hic-5 in tumors tissues compared with their normal counterparts in situ (**Figure 1B** for SD55, SD77, SD128, TS305, TS328, TS330 and Supplementary Figure 2 for SD12, SD13, SD28, SD78).

Hic-5 upregulated SNA transcriptional factor for mesenchymal gene expression and migration/invasion of patient-derived HCCs

Further, we set out to establish patient-derived metastatic HCCs with overexpression of Hic-5. Two of the established HCCs, namely HCC 374 (from patient TS330) and HCC372 (from patient TS328) cell lines (**Figure 2A**), which were authenticated by short-tandem repeat analysis (Supplementary Figure 1), were employed as models for Hic-5-based targeted therapy. As demonstrated in **Figure 2B** and **2C**, the expression of Hic-5 mRNA in HCC372 and HCC374 cells, respectively, was efficiently depleted by Hic-5 siRNA. Moreover, the depletion of Hic-5 in HCC372 (**Figure 2B**) and HCC374 (**Figure 2C**) cells greatly reduced the mRNA levels of SNA and its downstream mesenchymal genes, including MMP-9 and FN, which have been found to be positively regulated by Hic-5 in HCCs [14, 22]. Consistently, the depletion of Hic-5 and SNA inhibited the migration of HCC372 cells (**Figure 3A**) by 20-85% and 60-80%, respectively, in a dose-dependent manner. Moreover, 6.25 nM Hic-5 siRNA and 12.5 nM SNA siRNA additively suppressed the migration of HCC372 cells by 75% (**Figure 3A** and **3C**). Similarly, 12.5 and 25 nM of Hic-5 and SNA siRNA dose-dependently suppressed the migration of HCC374 cells by 35-85% and 55-80%, respectively (**Figure 3B** and **3D**). Moreover, 12.5 nM Hic-5 siRNA coupled with 25 nM SNA siRNA additively suppressed the migration of HCC374 cells by 60% (**Figure 3B** and **3D**). On the other hand, the invasiveness of HCC372 cells was inhibited by the depletion of both Hic-5 and SNA (Supplementary Figure 3, upper panel) whereas that of HCC374 cells was significantly decreased by the depletion of Hic-5 (Supplementary Figure 3, lower panel) but not SNA (data not shown). In addition, the depletion of

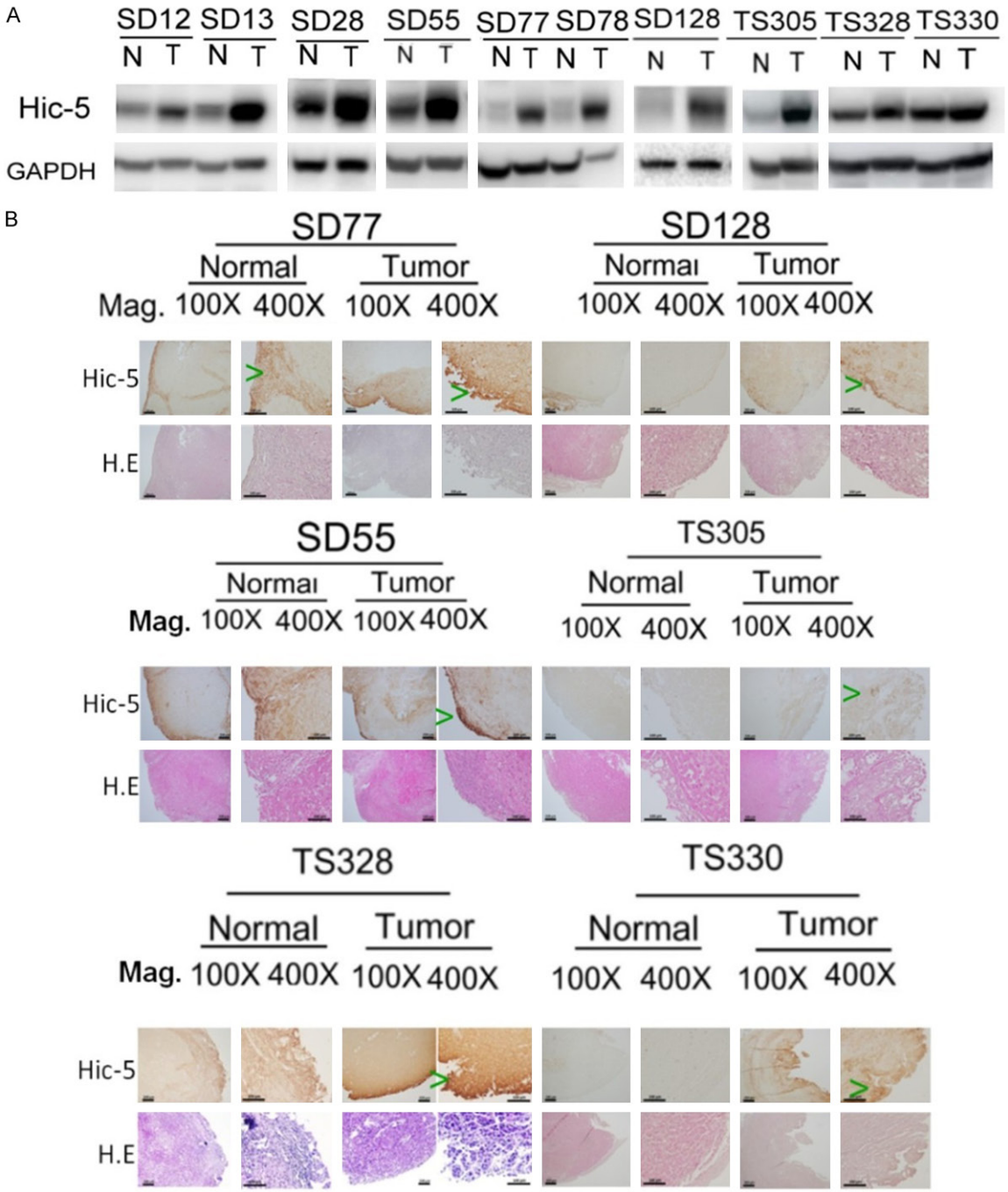

Figure 1. Western blot and IHC of Hic-5 in HCC tissues. A. Tissue lysates of tumor (T) coupled with the normal counterpart (N) of indicated HCCs were subjected to Western blot of Hic-5. GAPDH was included as an internal control. B. IHC of Hic-5 on tumor and normal counterpart of indicated HCCs. H.E. stains for each sample are included. Arrow head indicate the location of high Hic-5 staining region (brown color) in tumor section under 100- and 400-fold of magnification. The results shown were representatives of two reproducible data.

Hic-5 and SNA did not inhibit the growth of HCC372 and HCC374 cells using the MTT cell proliferation assay (data not shown). This finding excluded the possibility that the decrease in cell migration/invasion triggered by the depletion of Hic-5 and SNA was due to decreased cell growth. In summary, Hic-5 upregulated SNA for mesenchymal gene expression and migration/invasion in the newly established patient-derived HCCs.

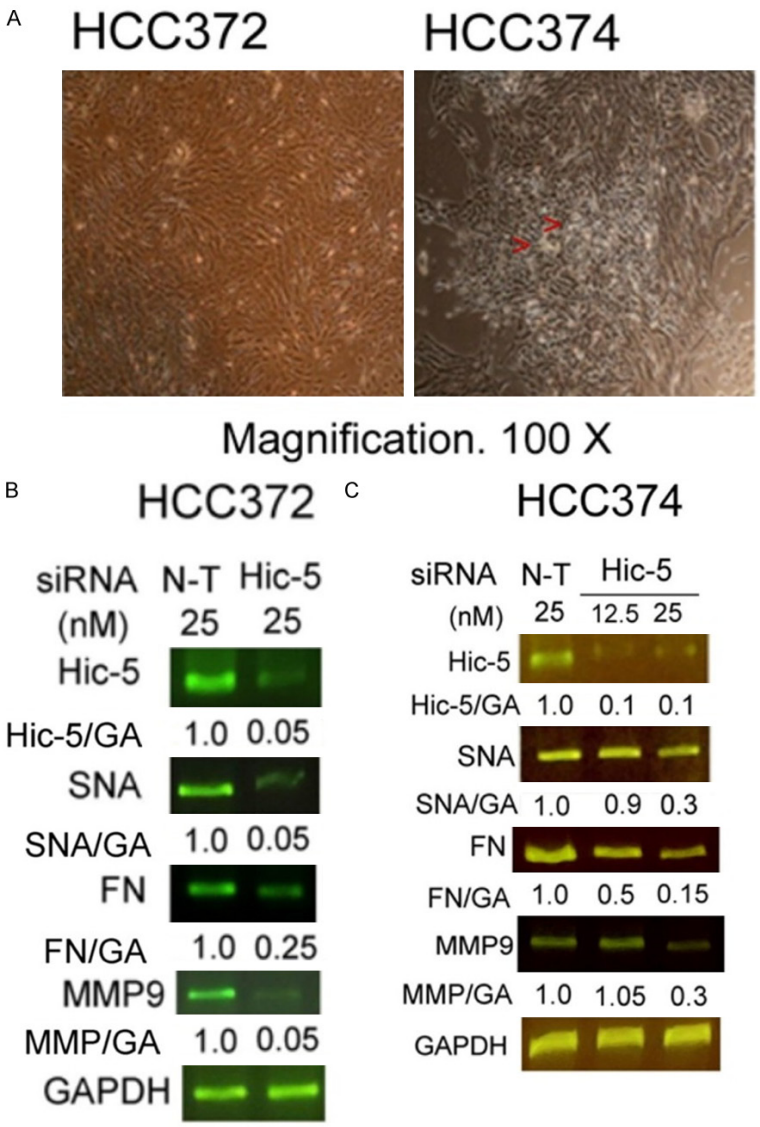

Figure 2. Establishment of patient-derived HCC and depletion of Hic-5 and SNA reduced expression of downstream metastasis-related genes in HCC 372. (A) Primary cultures of indicated patient-derived HCC cell lines were established according to standard method (feeder layer selection). Morphology of cells were pictured at 100× magnification. Red arrow heads showed the piled-up areas in HCC374. HCC372 (B) and HCC374 (C) cells were transfected with Hic-5 siRNA for 48 h at indicated concentrations. RT/PCR were performed using GAPDH as an internal control. The Non-targeting (N-T) siRNA groups are the negative control groups. In (B) and (C), GAPDH is an internal control. The numbers below each band are the relative intensities of the averages of three reproducible data of indicated molecules vs that of GAPDH (coefficients of variation, C.V. = 5%), taking the data of N-T as 1.0. The data shown are representative of three reproducible data.

Novel metastasis-related genes downstream of Hic-5 essential for HCC progression

We further explored the detailed molecular pathway for Hic-5-mediated HCC progression in order to search more potential targets. According to the results of whole-transcriptome mRNA sequencing, a total of 152 genes were differentially expressed in Hic-5-depleted cells. Of these, 127 genes were decreased and 25 were increased in Hic-5-depleted HCC372 cells compared with those in the non-targeting (N-T) siRNA-transfected cells (Supplementary Figure 4). These findings indicated that 127 and 25 genes were upregulated and downregulated by Hic-5, respectively (Supplementary Table 3). Among the genes upregulated by Hic-5 (Supplementary Table 4), two are potentially involved in metastasis, namely ROMO [23] and transcriptional factor ZNF395 [24] (marked in red in Supplementary Table 4). The upregulation of the two genes by Hic-5 was validated by the decrease of ROMO and ZNF395 (by 45% and 75%, respectively) in Hic-5-depleted HCC372 cells compared with the N-T siRNA-transfected cells using RT-PCR (**Figure 4A**). Importantly, the depletion of ROMO and ZNF395 (by 12.5 and 25 nM siRNA) suppressed the migration of HCC372 cells by 30-62% and 38-60%, respectively, in a dose-dependent manner (**Figure 4B**). Consistently, the depletion of ROMO (**Figure 4C**, left panel) and ZNF395 (**Figure 4C**, right panel) by 12.5 and 25 nM siRNA significantly decreased the expression of downstream mesenchymal genes, including MMP9 and FN by 90% and 50%, respectively. The knockdown efficiencies of siRNA for ROMO and ZNF395 demonstrated the decrease of the indicated mRNAs by 90% and 50% (**Figure 4C**, left and right panel, respectively). Interestingly,

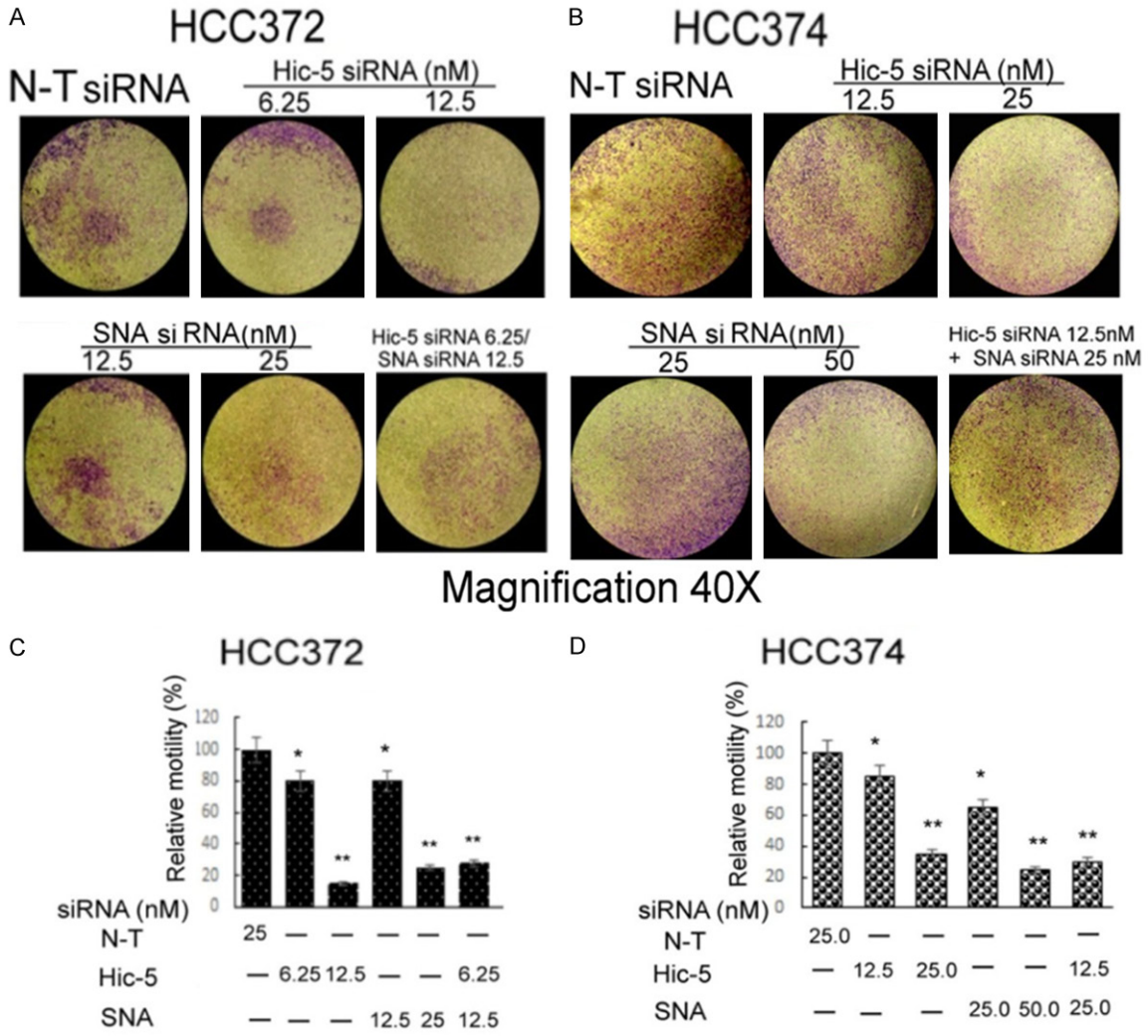

Figure 3. Depletion of Hic-5 and SNA suppressed migration of patient-derived HCCs. HCC372 (A), HCC374 (B) cells were transfected with Hic-5 and SNA siRNA at indicated concentrations (nM) for 48 h. Trans-well migration assays were performed. The images of crystal violet-stained migrated/invaded HCC cells were pictured under phase contrast microscope at 40× magnification. Non-targeting (N-T) siRNA is the negative control group. Quantitative figures (C) and (D) for (A) and (B), respectively, are shown below each crystal violet-stained image. Relative motility is calculated, taking the data of N-T group as 1.0. (*, **) represent the statistically significant difference ($P < 0.05$, $P < 0.01$, $N = 3$) between the indicated samples and N-T group.

knockdown of ROMO by 25 nM siRNA also suppressed Hic-5 expression at the mRNA level by 65% (**Figure 4C**, left panel), while knockdown of ZNF395 didn't (**Figure 4C**, right panel), implying a positive cross-talk between ROMO and Hic-5. Also, we examined the up and down relationship between SNA and ZNF395, the two oncogenic transcription factors upregulated through the Hic-5-mediated pathway. As demonstrated in **Figure 4A** (right panel), the depletion of SNA led to a decrease in the expression of ZNF395 by 70%, whereas depletion of ZNF395 did not exert suppressive effect on SNA (data not shown), suggesting that ZNF395 is downstream of SNA. Collectively, these results suggested that both ROMO and ZNF395 play important roles in mediating Hic-5-triggered pathway for migration of HCC372. We further examined whether both ROMO and ZNF395 were also regulated by Hic-5 in the other patient-derived HCC, HCC374. However, depletion of Hic-5 reduced the expression of ZNF395 but not ROMO (Supplementary Figure 5A). Consistently, depletion of ZNF395 (Supplementary Figure 5C) but not ROMO (data not shown) inhibit HCC374 migration by 60%.

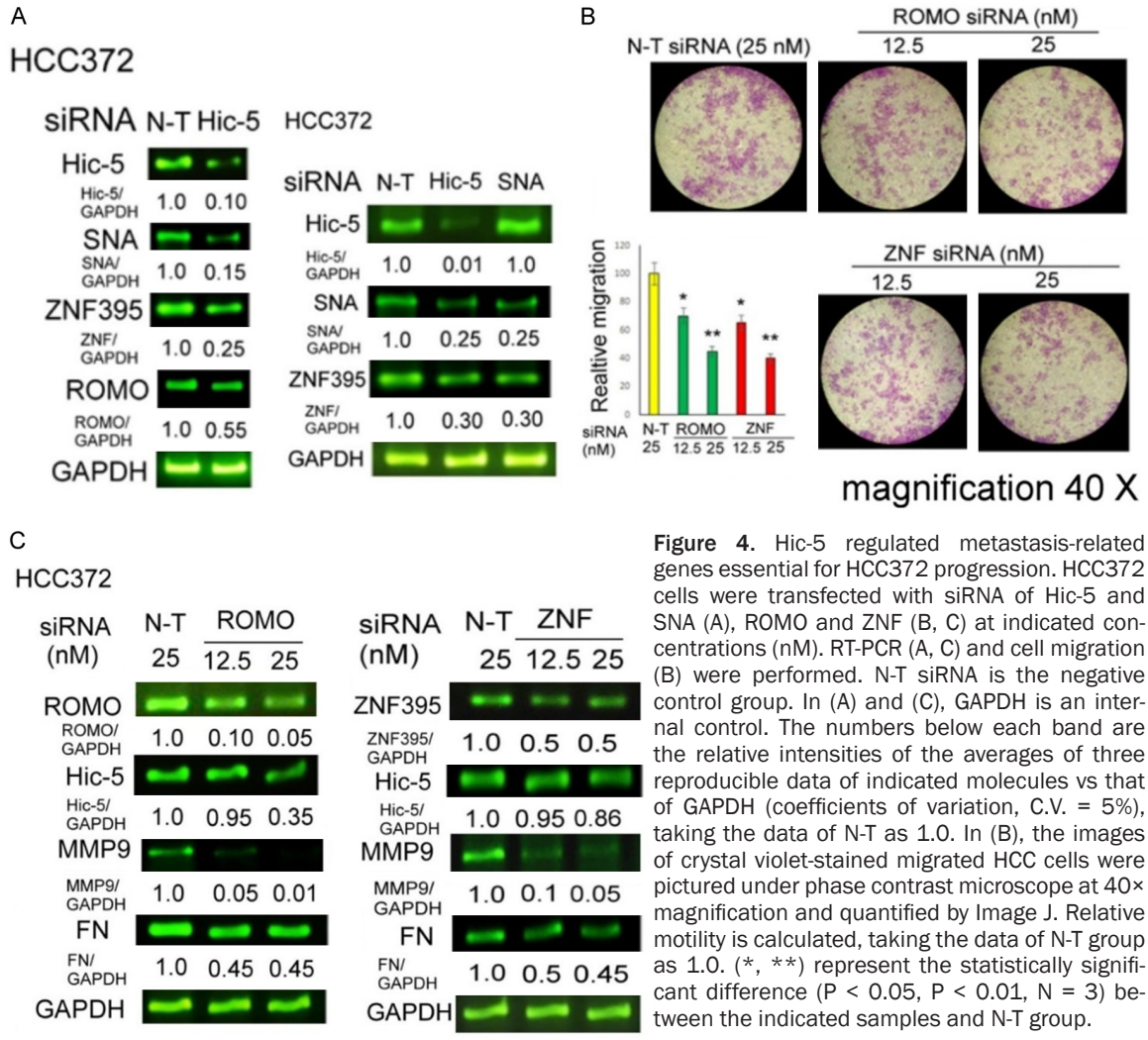

Figure 4. Hic-5 regulated metastasis-related genes essential for HCC372 progression. HCC372 cells were transfected with siRNA of Hic-5 and SNA (A), ROMO and ZNF (B, C) at indicated concentrations (nM). RT-PCR (A, C) and cell migration (B) were performed. N-T siRNA is the negative control group. In (A) and (C), GAPDH is an internal control. The numbers below each band are the relative intensities of the averages of three reproducible data of indicated molecules vs that of GAPDH (coefficients of variation, C.V. = 5%), taking the data of N-T as 1.0. In (B), the images of crystal violet-stained migrated HCC cells were pictured under phase contrast microscope at 40× magnification and quantified by Image J. Relative motility is calculated, taking the data of N-T group as 1.0. (*, **) represent the statistically significant difference ($P < 0.05$, $P < 0.01$, $N = 3$) between the indicated samples and N-T group.

On the other hand, depletion of ZNF395 effectively suppressed the mRNA of SNA (at 50 nM) and MMP9 (at 25 and 50 nM) but not FN (Supplementary Figure 5B). Thus, ZNF395 (but not ROMO) was also upregulated by Hic-5 for HCC374 migration.

ROMO was required in the Hic-5-mediated ROS signal pathway for the migration of HCC372 cells

As its name implies, reactive oxygen species modulator (ROMO) is a key regulator of ROS released from mitochondria [25]. ROMO was also well-known to play an essential role in the progression of tumors, including HCC [26-28] and gastric cancer [29] through the production of ROS. On the other hand, it was established that Hic-5 triggers metastasis *via* cross-talk with ROS signaling responsible for promoting HCC progression [13, 14, 30]. Therefore, it is reasonable to investigate whether ROMO is involved in Hic-5-mediated ROS signaling in HCC372. Initially, we found that DTT (0.5-2.0 mM) (a ROS scavenger) inhibited the expression of Hic-5, SNA and MMP9 at the mRNA level in a dose-dependent manner (**Figure 5A**). Consistently, 0.5-2.0 mM DTT suppressed the migration of HCC372 cells by 20-82% in a dose-dependent manner (**Figure 5B**, upper and lower left panel). In addition, cell proliferation was slightly decreased in the same concentration range (**Figure 5B**, lower right panel). Remarkably, using DCF-DA as a probe, the depletion of both Hic-5 and ROMO significantly reduced the total ROS generation by 55% and 43%, respectively (**Figure 5C**). Collectively, these results suggested that ROMO is involved in Hic-5-mediated ROS signaling, required for the progression of HCC.

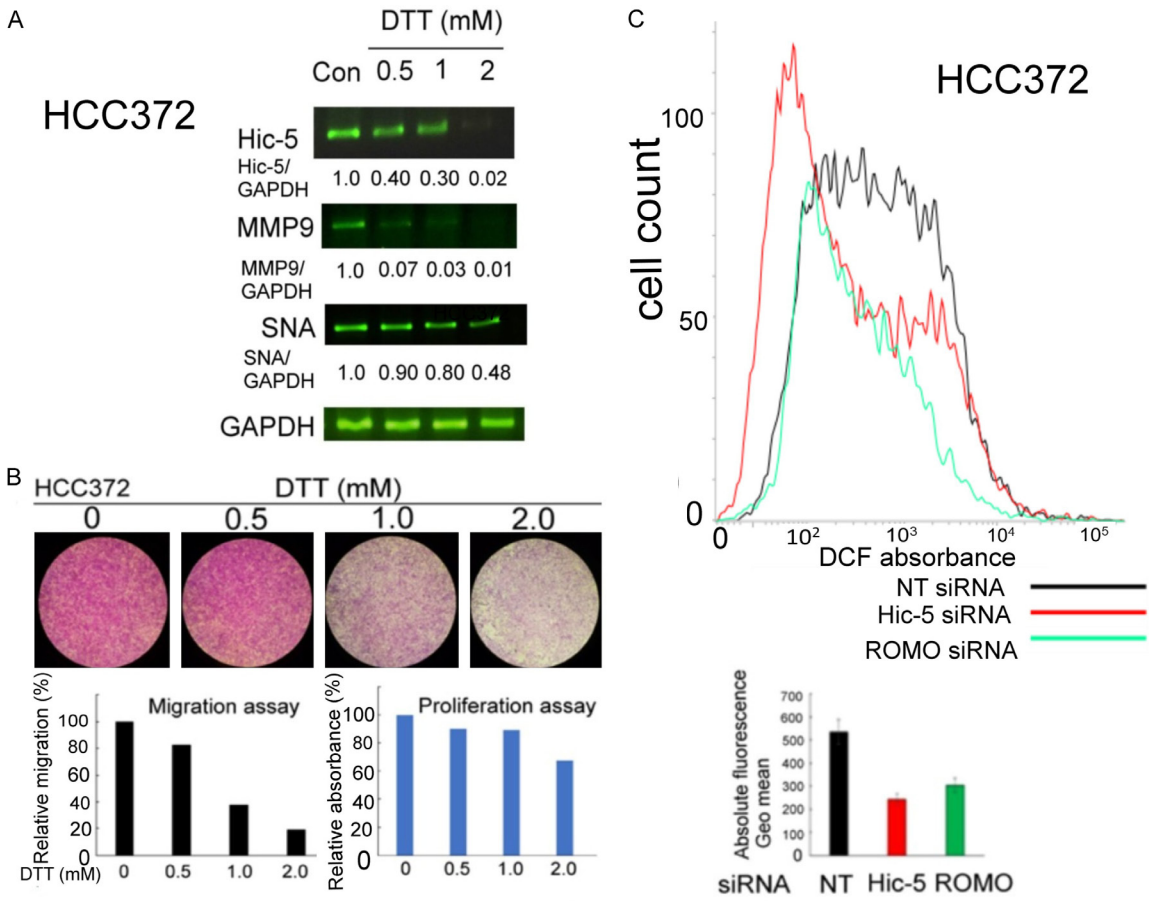

Figure 5. ROS scavenger suppress ROS signaling and downstream metastatic genes for cell migration whereas depletion of Hic-5 and ROMO decreased ROS generation in HCC372. HCC372 cells were treated with DTT at indicated concentrations (nM) (A) and transfected with Hic-5 or ROMO siRNA (B, C). RT-PCR (A), cell migration/proliferation (B) and ROS assay (C) were performed. Non-targeting (N-T) siRNA is the negative control group. In (A), GAPDH serves as an internal control. The numbers below each band are the relative intensities of the averages of three reproducible data of indicated molecules vs that of GAPDH (coefficients of variation, C.V. = 5%), taking the data of N-T as 1.0. In (B), the images of crystal violet-stained migrated HCC cells were pictured under phase contrast microscope at 40× magnification and quantified as blow by Image J. software (version 1.50 i). Relative cellular proliferation (by MTT assay) were represented in the lower right panel. In (C), ROS assay using DCFDA as a probe was quantified by flowcytometry, represented as absolute fluorescent G mean at 418 nm. The merged curves of Hic-5 or ROMO knockdown and N-T groups was shown in the right panel.

Suppression of Hic-5 by SNALP-Hic-5si inhibited the progression of HCC in vivo

For the establishment of targeted therapy aiming at Hic-5, we set out to perform *in vivo* knockdown of Hic-5 using Hic-5siRNA carried by SNALP nanoparticle (SNALP-Hic-5si). Initially, HCC372 and HCC374 cells were subcutaneously inoculated into the flanks of SCID mice for the development of tumors (diameter: 1 cm), which were subsequently equally divided and orthotropically transplanted into the middle lobe of the liver of mice. After 1 week, SNALP-Hic-5si or SNALP-empty (SNALP without any siRNA incorporated) was administered *via* tail-vein injection twice weekly. Six weeks after the administration of the nanoparticles, the mice were sacrificed for examining the development of HCCs. Remarkably, HCC372 (**Figure 6A**) and HCC374 (**Figure 6B**) tumors that developed in the liver of mice injected with SNALP-Hic-5si were markedly suppressed by 80-90% compared with those in mice treated with SNALP-empty ($P < 0.008$, $n = 3$ for each tumor). Hematoxylin-eosin staining of tumor tissues demonstrated that a mixed pseudo-glandular (blue ellipse) and poorly differentiated (red rectangle) pattern was observed on the tissue section of HCC from mice treated with SNALP-empty (**Figure 6E**, upper panel), however, only

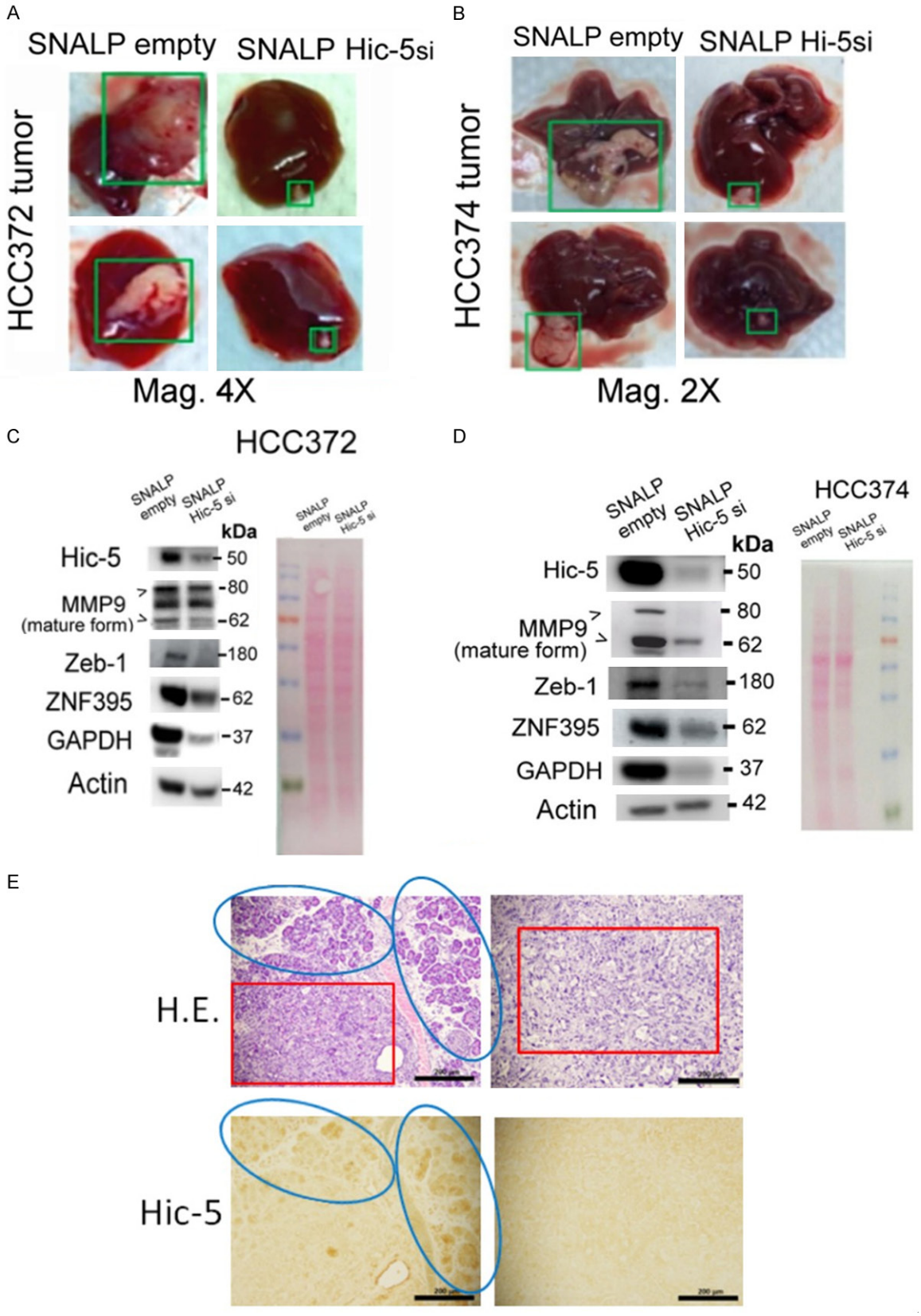

Figure 6. In vivo knockdown of Hic-5 suppressed progression of HCC372 and HCC374 in SCID mice liver. HCC372 (A) and HCC 374 (B) cells were inoculated on both right and left flanks of SCID mice for one month. The tumors cut in small pieces were transplanted on middle lobe of liver. After one week the SNALP-carried Hic-5 siRNA (50 mg siRNA/

kg mouse) or SNALP SNALP-empty was injected *via* tail vein twice a week until 1.5 month. The mice were sacrificed and the liver of HCC372/HCC374 tumor were taken and pictured (with 2 and 4-fold magnification for HCC372 and HCC374, respectively). The results shown were representatives of three reproducible data. Western of Hic-5 and the indicated downstream genes in HCC372 (C) and HCC374 (D) tumors from liver of mice administrated with SNALP-carried Hic-5 siRNA or SNALP-empty. Ponceau S stain for each blot were shown as loading control. In H.E. stains (E) for each parallel section of SNALP-Hic-5 siRNA and SNALP-empty group (upper panel), blue ellipse encloses the pseudoglandular pattern in HCCs whereas red rectangle marked the poorly-differentiated pattern. Lower panel demonstrated IHC of Hic-5 on tumor sections of liver from mice with SNALP-carried Hic-5 siRNA or SNALP-empty. The deep-brown color of the Hic-5 staining region localized in pseudoglandular but not poorly-differentiated loci.

the poorly differentiated pattern was observed on that of the SNALP-Hic-5si group (**Figure 6E**, upper panel). Interestingly, IHC analysis of Hic-5 revealed high Hic-5 expression in the pseudo-glandular loci, but not in the poorly differentiated loci on tissue sections from mice treated with SNALP-empty (**Figure 6E**, lower panel). In contrast, Hic-5 expression was not detected on that of SNALP-Hic-5si group which exhibited only the poorly differentiated pattern (**Figure 6E**, lower panel). At the molecular level, the efficiency of SNALP-Hic-5si for *in vivo* knockdown was validated by western blotting, showing a drastic decrease in Hic-5 levels (by 90%) in tissues of HCC372 (**Figure 6C**) and HCC374 (**Figure 6D**) tumors obtained from mice treated with SNALP-Hic-5si *versus* SNALP-empty group. Consistently, the depletion of Hic-5 in HCC372 (**Figure 6C**) and HCC374 (**Figure 6D**) tumors was accompanied by a marked decrease (80-95%) in the expression of downstream genes, including ZNF395, MMP9, and Zeb-1 (another downstream mesenchymal gene of Hic-5 [14]). Surprisingly, the level of glyceraldehyde-3-phosphate dehydrogenase (GAPDH), one of the commonly used internal controls, was also drastically decreased in HCC372 and HCC374 tumors resected from mice treated with SNALP-Hic-5si (**Figure 6C** and **6D**). The expression of β-actin (another common internal marker) was also significantly decreased in HCC372 (but not HCC374) tumors from mice treated with SNALP-Hic-5si. To exclude the possibility of protein loading error, we performed Ponceau S staining of the western blots. The results confirmed that an equal amount of protein from each sample was loaded (**Figure 6C** and **6D**, right panel). Thus, GAPDH, known to play an essential role in enhanced glycolysis and energy production, may be required for the progression of HCC mediated by Hic-5, consistent with the Warburg effect [31], which is an issue worthy of further investigation. Taken together, *in vivo* depletion of Hic-5 by SNALP-carried Hic-5siRNA can prevent the progression of two patient-derived HCCs coupled with the suppression of Hic-5 downstream genes.

Discussion

The challenges and alternative strategies in targeted therapy of HCC

In the past decades, the complex mechanisms (including EMT/migration, immune escape, and angiogenesis/colony formation) in metastasis have been intensively studied [6]. In the tumor microenvironment, cross talks between primary HCC and stromal cells result in the secretion of numerous growth factors and cytokines capable of triggering EMT, migration, and invasion of HCC cells. Moreover, the receptors of metastatic factors on tumor cells are often upregulated, resulting in deregulation of the signaling pathway. Thus, blockade of deregulated signaling, such as those triggered by receptor tyrosine kinases (RTKs), including epidermal growth factor receptor (EGFR) [32, 33] and MET [34], appears to be a promising therapeutic strategy [35]. However, the therapies targeting RTKs remain unsatisfactory thus far. For example, the use of Sorafenib (the first multi-tyrosine kinase inhibitor approved for the treatment of HCC) often led to the development of resistance in most patients with HCC [36]. In addition, many tyrosine kinase inhibitors may affect the physiological functions of RTKs in non-tumor organs, thereby causing toxicity and off-target effects (e.g., cardiotoxicity, hypertension, and proteinuria) [37-39]. Recently, anti-metastatic strategies were shifted toward targeting different factors involved in the metastatic pathway. In this study, we recognized Hic-5 as a promising therapeutic target for preventing HCC progression both *in vitro* and *in vivo* (**Figures 3** and **6**). Moreover, we identified two of the metastasis-related genes downstream of Hic-5 (ie, ROMO and ZNF395), which are potentially involved in HCC progres-

sion (**Figure 4**). Accordingly, they may also be potential therapeutic targets.

ROMO mediated Hic-5-ROS signaling for the progression of HCC

ROMO is a mitochondrial protein cloned in 2006 from cancer tissues involved in resistance to chemotherapy [40]. Recent reports demonstrated that ROMO is a constituent of translocase (TIM23) within the inner mitochondrial membrane regulating the assembly of the oxidative phosphorylation machinery [41] and playing a pivotal role in the regulation of mitochondrial structure integrity [42]. Moreover, ROMO is a key regulator of ROS released from mitochondria [25] involved in cancer progression. In this study, we found a cross-talk between ROMO and Hic-5 in HCC372, thereby mediating the expression of mesenchymal genes (**Figure 4A**, **4C**) and ROS generation (**Figure 5C**). Thus, it is interesting to investigate the mechanism by which ROMO and Hic-5 cooperate to regulate ROS signaling in HCC-372. However, since ROMO was not positively regulated by Hic-5 in HCC374 (Supplementary Figure 5A) as in HCC372 (**Figure 4A**) the crosstalk of ROMO with Hic-5 for ROS signaling may be context-dependent due to heterogeneity of HCC. Whether ROMO is associated with the progression of some Hic-5-overexpressing HCCs is worthy of further investigation.

ZNF395 participated in the transcriptional system for Hic-5-mediated HCC progression

Previously, the role of SNA in upregulating the expression of mesenchymal genes for EMT and cell migration in HCC has been established by our [22] and other groups [43]. In this study, we also found another Hic-5-upregulated transcriptional factor, ZNF395, located downstream of SNA. ZNF395 is ubiquitously expressed, and has been identified as a common transcription factor involved in several cellular responses, including carcinogenesis [44]. Numerous reports reveal that ZNF395 plays an oncogenic role and is overexpressed in various types of cancers, including glioblastoma, kidney cancer, osteosarcoma, and chondrosarcoma [24]. In this study, we showed that ZNF395 was required for the expression of mesenchymal genes (**Figure 4C**, right panel) and migration of HCC372 cells (**Figure 4B**) and greatly decreased in HCCs in livers of SCID mice depleted of Hic-5 (**Figure 6C**, **6D**). These imply it participate in the transcriptional system for Hic-5-mediated HCC progression.

In vivo targeting of Hic-5 using a nanoparticle-based siRNA technique

Since the discovery of siRNA in 1998, multiple studies have demonstrated its use in the treatment of cancers, including HCC [45]. Specifically, targeting the metastatic genes (e.g., heparanase-1 (HSPE1) [46] and urokinase-type plasminogen activator (uPAR) [47] using siRNA may prevent HCC progression. However, *in vitro* RNA interference was used in these studies; hence, their results should be validated *in vivo*. Recently, several reports demonstrated great advances in the design of nanoparticle systems, including lipid-, polymer-, or virus-based nano-carriers for the *in vivo* delivery of siRNAs in HCC [48]. Among the lipid-based nano-carriers, SNALP holds considerable promise. Previously, SNALP was used for the systemic delivery of siRNA for the modulator of ubiquitination [49] to suppress liver cancer without immune responses. Moreover, SNALP containing the siRNA targeting cell division cycle associated 1 (CDCA1) inhibited tumor growth in orthotropic Huh-7 HCC models without induction of liver toxicity, including changes in the liver color and elevation in the levels of alanine aminotransferase and aspartate transaminase [50]. In this study, we also used SNALP-Hic-5si to successfully suppress the development of orthotropic patient-derived HCCs in SCID mice (**Figure 6A**, **6B**) without liver toxicity (data not shown). Importantly, the efficacy of SNALP-Hic-5si for the *in vivo* depletion of Hic-5 and suppression of the downstream genes of Hic-5, such as ZNF395, MMP9, and Zeb-1, was validated (**Figure 6C**, **6D**).

Conclusions

We delineated the Hic-5-mediated molecular pathway for the migration/invasion in HCCs, and established an *in vivo* Hic-5 knockdown strategy for preventing the progression of patient-derived HCCs. Moreover, the novel Hic-5-regulated genes identified in this study, namely ZNF395 and ROMO, may also be employed as therapeutic targets. This approach can be adopted as a promising targeted therapy against the progression of HCCs with overexpression of Hic-5.

Acknowledgements

We are thankful for the support of the study by Tzu Chi Research Department (TCRD) (grant number: TCRD111-079); and a collaborative grant by Tzu Chi Medical Foundation (Tzu Chi University) and Academia Sinica awarded to Wen-Sheng Wu (grant number: TCAS-111-02). We also thank Ms. Shu-Chuan Lin for establishing the patient-derived HCC cell lines.

Disclosure of conflict of interest

None.

Address correspondence to: Yen-Cheng Chen, School of Medicine, Tzu Chi University, No. 701 Zhongyang Road, Section 3, Hualien 97004, Taiwan. Tel: +886-038561825 Ext. 15829; E-mail: yccmdsurg@gms.tcu.edu.tw

References

[1] Global Burden of Disease Liver Cancer Collaboration, Akinyemiju T, Abera S, Ahmed M, Alam N, Alemayohu MA, Allen C, Al-Raddadi R, Alvis-Guzman N, Amoako Y, Artaman A, Ayele TA, Barac A, Bensenor I, Berhane A, Bhutta Z, Castillo-Rivas J, Chitheer A, Choi JY, Cowie B, Dandona L, Dandona R, Dey S, Dicker D, Phuc H, Ekwueme DU, Zaki MS, Fischer F, Fürst T, Hancock J, Hay SI, Hotez P, Jee SH, Kasaeian A, Khader Y, Khang YH, Kumar A, Kutz M, Larson H, Lopez A, Lunevicius R, Malekzadeh R, McAlinden C, Meier T, Mendoza W, Mokdad A, Moradi-Lakeh M, Nagel G, Nguyen Q, Nguyen G, Ogbo F, Patton G, Pereira DM, Pourmalek F, Qorbani M, Radfar A, Roshandel G, Salomon JA, Sanabria J, Sartorius B, Satpathy M, Sawhney M, Sepanlou S, Shackelford K, Shore H, Sun J, Mengistu DT, Topór-Mądry R, Tran B, Ukwaja KN, Vlassov V, Vollset SE, Vos T, Wakayo T, Weiderpass E, Werdecker A, Yonemoto N, Younis M, Yu C, Zaidi Z, Zhu L, Murray CJL, Naghavi M and Fitzmaurice C. The burden of primary liver cancer and underlying etiologies from 1990 to 2015 at the global, regional, and national level: results from the global burden of disease study 2015. JAMA Oncol 2017; 3: 1683-1691.

[2] Tang ZY, Yu YQ, Zhou XD, Ma ZC and Wu ZQ. Progress and prospects in hepatocellular carcinoma surgery. Ann Chir 1998; 52: 558-563.

[3] Lin YL and Li Y. Study on the hepatocellular carcinoma model with metastasis. Genes Dis 2020; 7: 336-350.

[4] Valastyan S and Weinberg RA. Tumor metastasis: molecular insights and evolving paradigms. Cell 2011; 147: 275-292.

[5] Quail DF and Joyce JA. Microenvironmental regulation of tumor progression and metastasis. Nat Med 2013; 19: 1423-1437.

[6] Ganesh K and Massagué J. Targeting metastatic cancer. Nat Med 2021; 27: 34-44.

[7] Saxena S and Singh RK. Chemokines orchestrate tumor cells and the microenvironment to achieve metastatic heterogeneity. Cancer Metastasis Rev 2021; 40: 447-476.

[8] Shibanuma M, Mashimo J, Kuroki T and Nose K. Characterization of the TGF beta 1-inducible hic-5 gene that encodes a putative novel zinc finger protein and its possible involvement in cellular senescence. J Biol Chem 1994; 269: 26767-26774.

[9] Nishiya N, Iwabuchi Y, Shibanuma M, Côté JF, Tremblay ML and Nose K. Hic-5, a paxillin homologue, binds to the protein-tyrosine phosphatase PEST (PTP-PEST) through its LIM 3 domain. J Biol Chem 1999; 274: 9847-9853.

[10] Petropoulos C, Oddou C, Emadali A, Hiriart-Bryant E, Boyault C, Faurobert E, Vande Pol S, Kim-Kaneyama JR, Kraut A, Coute Y, Block M, Albiges-Rizo C and Destaing O. Roles of paxillin family members in adhesion and ECM degradation coupling at invadosomes. J Cell Biol 2016; 213: 585-599.

[11] Goreczny GJ, Ouderkirk-Pecone JL, Olson EC, Krendel M and Turner CE. Hic-5 remodeling of the stromal matrix promotes breast tumor progression. Oncogene 2017; 36: 2693-2703.

[12] Omoto T, Kim-Kaneyama JR, Lei XF, Orimo A, Ohnishi K, Yoshihara K, Miyauchi A, Li S, Gao L, Umemoto T, Tanaka J, Nakahara K, Takeya M, Ishida F, Kudo SE, Haraguchi S, Miyazaki T and Miyazaki A. The impact of stromal Hic-5 on the tumorigenesis of colorectal cancer through lysyl oxidase induction and stromal remodeling. Oncogene 2018; 37: 1205-1219.

[13] Wu JR, Hu CT, You RI, Pan SM, Cheng CC, Lee MC, Wu CC, Chang YJ, Lin SC, Chen CS, Lin TY and Wu WS. Hydrogen peroxide inducible clone-5 mediates reactive oxygen species signaling for hepatocellular carcinoma progression. Oncotarget 2015; 6: 32526-32544.

[14] Wu JR, You RI, Hu CT, Cheng CC, Rudy R and Wu WS. Hydrogen peroxide inducible clone-5 sustains NADPH oxidase-dependent reactive oxygen species-c-jun N-terminal kinase signaling in hepatocellular carcinoma. Oncogenesis 2019; 8: 40.

[15] Noguchi F, Inui S, Nakajima T and Itami S. Hic-5 affects proliferation, migration and invasion of B16 murine melanoma cells. Pigment Cell Melanoma Res 2012; 25: 773-782.

[16] Mandal JP, Shiue CN, Chen YC, Lee MC, Yang HH, Chang HH, Hu CT, Liao PC, Hui LC, You RI and Wu WS. PKCδ mediates mitochondrial ROS generation and oxidation of HSP60 to relieve RKIP inhibition on MAPK pathway for HCC

progression. Free Radic Biol Med 2021; 163: 69-87.
[17] Jena MK and Janjanam J. Role of extracellular matrix in breast cancer development: a brief update. F1000Res 2018; 7: 274.
[18] Wu WS. The role of hydrogen peroxide-inducible clone-5 in tumor progression. Ci Ji Yi Xue Za Zhi 2020; 32: 1-4.
[19] Qian B, Wei L, Yang Z, He Q, Chen H, Wang A, Yang D, Li Q, Li J, Zheng S and Fu W. Hic-5 in pancreatic stellate cells affects proliferation, apoptosis, migration, invasion of pancreatic cancer cells and postoperative survival time of pancreatic cancer. Biomed Pharmacother 2020; 121: 109355.
[20] Craig AJ, von Felden J, Garcia-Lezana T, Sarcognato S and Villanueva A. Tumour evolution in hepatocellular carcinoma. Nat Rev Gastroenterol Hepatol 2020; 17: 139-152.
[21] Li L, Wang R, Wilcox D, Sarthy A, Lin X, Huang X, Tian L, Dande P, Hubbard RD, Hansen TM, Wada C, Zhao X, Kohlbrenner WM, Fesik SW and Shen Y. Developing lipid nanoparticle-based siRNA therapeutics for hepatocellular carcinoma using an integrated approach. Mol Cancer Ther 2013; 12: 2308-2318.
[22] Ly TM, Chen YC, Lee MC, Hu CT, Cheng CC, Chang HH, You RI and Wu WS. Snail upregulates transcription of FN, LEF, COX2, and COL1A1 in hepatocellular carcinoma: a general model established for snail to transactivate mesenchymal genes. Cells 2021; 10: 2202.
[23] Ghasemi H, Amini MA, Pegah A, Azizi E, Tayebinia H, Khanverdilou S, Mousavibahar SH and Alizamir A. Overexpression of reactive oxygen species modulator 1 is associated with advanced grades of bladder cancer. Mol Biol Rep 2020; 47: 6497-6505.
[24] Chen C, Zhou H, Liu Z and Ma X. Dysregulation of zinc finger protein 395 contributes to the pathogenesis of chondrosarcoma. Onco Targets Ther 2021; 14: 3545-3553.
[25] Norton M, Ng AC, Baird S, Dumoulin A, Shutt T, Mah N, Andrade-Navarro MA, McBride HM and Screaton RA. ROMO1 is an essential redox-dependent regulator of mitochondrial dynamics. Sci Signal 2014; 7: ra10.
[26] Chung JS, Park S, Park SH, Park ER, Cha PH, Kim BY, Chung YM, Woo SR, Han CJ, Kim SB, Suh KS, Jang JJ, Lee K, Choi DW, Lee S, Lee GY, Hahm KB, Shin JA, Kim BS, Noh KH, Kim TW, Lee KH and Yoo YD. Overexpression of Romo1 promotes production of reactive oxygen species and invasiveness of hepatic tumor cells. Gastroenterology 2012; 143: 1084-1094, e7.
[27] Chung JS, Lee S and Yoo YD. Constitutive NF-κB activation and tumor-growth promotion by Romo1-mediated reactive oxygen species production. Biochem Biophys Res Commun 2014; 450: 1656-1661.
[28] Lee S, Park YH, Chung JS and Yoo YD. Romo1 and the NF-κB pathway are involved in oxidative stress-induced tumor cell invasion. Int J Oncol 2015; 46: 2021-2028.
[29] Amini MA, Karimi J, Khodadadi I, Tavilani H, Talebi SS and Afshar B. Overexpression of ROMO1 and OMA1 are potentially biomarkers and predict unfavorable prognosis in gastric cancer. J Gastrointest Cancer 2020; 51: 939-946.
[30] Wu WS. The signaling mechanism of ROS in tumor progression. Cancer Metastasis Rev 2006; 25: 695-705.
[31] Tang Z, Yuan S, Hu Y, Zhang H, Wu W, Zeng Z, Yang J, Yun J, Xu R and Huang P. Over-expression of GAPDH in human colorectal carcinoma as a preferred target of 3-bromopyruvate propyl ester. J Bioenerg Biomembr 2012; 44: 117-125.
[32] Khan K, Valeri N, Dearman C, Rao S, Watkins D, Starling N, Chau I and Cunningham D. Targeting EGFR pathway in metastatic colorectal cancer- tumour heterogeniety and convergent evolution. Crit Rev Oncol Hematol 2019; 143: 153-163.
[33] London M and Gallo E. Epidermal growth factor receptor (EGFR) involvement in epithelial-derived cancers and its current antibody-based immunotherapies. Cell Biol Int 2020; 44: 1267-1282.
[34] Liu X, Sun R, Chen J, Liu L, Cui X, Shen S, Cui G, Ren Z and Yu Z. Crosstalk mechanisms between HGF/c-Met axis and ncRNAs in malignancy. Front Cell Dev Biol 2020; 8: 23.
[35] Wang H and Chen L. Tumor microenviroment and hepatocellular carcinoma metastasis. J Gastroenterol Hepatol 2013; 28 Suppl 1: 43-48.
[36] Fornari F, Giovannini C, Piscaglia F and Gramantieri L. Elucidating the molecular basis of sorafenib resistance in HCC: current findings and future directions. J Hepatocell Carcinoma 2021; 8: 741-757.
[37] Kaur J, Tuler S and Dasanu CA. Sustained erythrocytosis due to the use of Lenvatinib. J Oncol Pharm Pract 2022; 28: 475-478.
[38] van Elst JM, IJzerman NS, Mathijssen RHJ, Steeghs N, Reyners AKL and de Haan JJ. Taste, smell and mouthfeel disturbances in patients with gastrointestinal stromal tumors treated with tyrosine-kinase inhibitors. Support Care Cancer 2022; 30: 2307-2315.
[39] Farghaly TA, Al-Hasani WA and Abdulwahab HG. An updated patent review of VEGFR-2 inhibitors (2017-present). Expert Opin Ther Pat 2021; 31: 989-1007.

[40] Chung YM, Kim JS and Yoo YD. A novel protein, Romo1, induces ROS production in the mitochondria. Biochem Biophys Res Commun 2006; 347: 649-655.
[41] Richter F, Dennerlein S, Nikolov M, Jans DC, Naumenko N, Aich A, MacVicar T, Linden A, Jakobs S, Urlaub H, Langer T and Rehling P. ROMO1 is a constituent of the human presequence translocase required for YME1L protease import. J Cell Biol 2019; 218: 598-614.
[42] Bae YS, Oh H, Rhee SG and Yoo YD. Regulation of reactive oxygen species generation in cell signaling. Mol Cells 2011; 32: 491-509.
[43] Wang Y, Shi J, Chai K, Ying X and Zhou BP. The role of snail in EMT and tumorigenesis. Curr Cancer Drug Targets 2013; 13: 963-972.
[44] Laity JH, Lee BM and Wright PE. Zinc finger proteins: new insights into structural and functional diversity. Curr Opin Struct Biol 2001; 11: 39-46.
[45] Hajiasgharzadeh K, Somi MH, Shanehbandi D, Mokhtarzadeh A and Baradaran B. Small interfering RNA-mediated gene suppression as a therapeutic intervention in hepatocellular carcinoma. J Cell Physiol 2019; 234: 3263-3276.
[46] Yu SJ, Kang XH, Zhang JN, Wang HM, Xie T, Wang W and Wang SJ. Effects of small interfering RNA targeting heparanase-1 combined with heparin on invasiveness of mouse hepatocellular carcinoma cell lines. Chin J Cancer 2010; 29: 816-823.
[47] Salvi A, Arici B, De Petro G and Barlati S. Small interfering RNA urokinase silencing inhibits invasion and migration of human hepatocellular carcinoma cells. Mol Cancer Ther 2004; 3: 671-678.
[48] Varshosaz J and Farzan M. Nanoparticles for targeted delivery of therapeutics and small interfering RNAs in hepatocellular carcinoma. World J Gastroenterol 2015; 21: 12022-12041.
[49] Lee YH, Andersen JB, Song HT, Judge AD, Seo D, Ishikawa T, Marquardt JU, Kitade M, Durkin ME, Raggi C, Woo HG, Conner EA, Avital I, Maclachlan I, Factor VM and Thorgeirsson SS. Definition of ubiquitination modulator COP1 as a novel therapeutic target in human hepatocellular carcinoma. Cancer Res 2010; 70: 8264-8269.
[50] Wei BR, Hoover SB, Peer CJ, Dwyer JE, Adissu HA, Shankarappa P, Yang H, Lee M, Peat TJ, Figg WD and Simpson RM. Efficacy, tolerability, and pharmacokinetics of combined targeted MEK and dual mTORC1/2 inhibition in a preclinical model of mucosal melanoma. Mol Cancer Ther 2020; 19: 2308-2318.

Supplementary Data

STR analysis for HCC372

- STR loci genotype ：

Locus Name	D5S818	D13S317	D7S820	D16S539	vWA	TH01	AMEL	TPOX	CSF1PO
Allele genotype	9,11	8,13	8,8	9,11	14,18	6,9	x,x	8,8	11,12

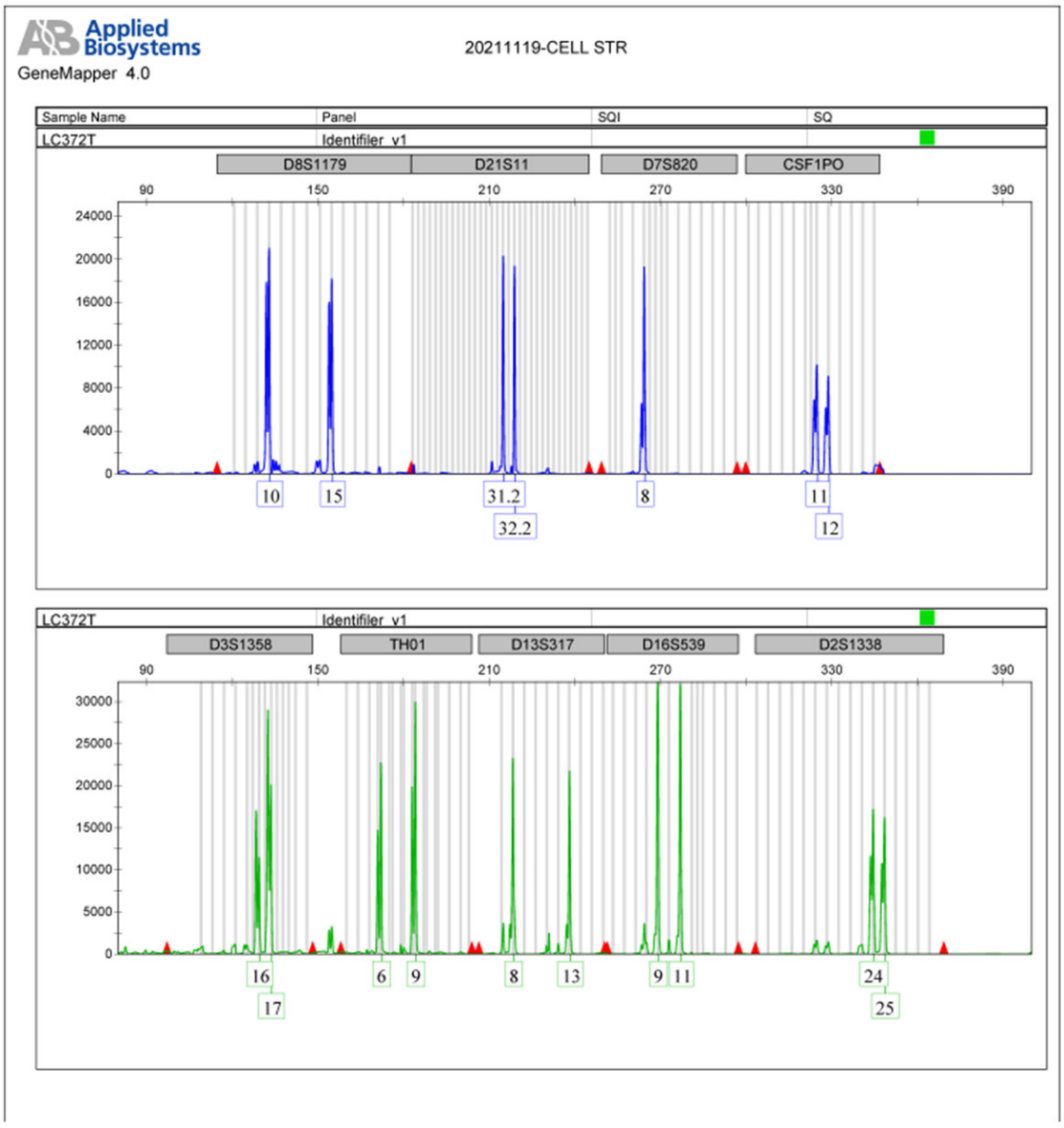

Applied Biosystems
GeneMapper 4.0

20211119-CELL STR

Sample Name	Panel	SQI	SQ
LC372T	Identifiler v1		

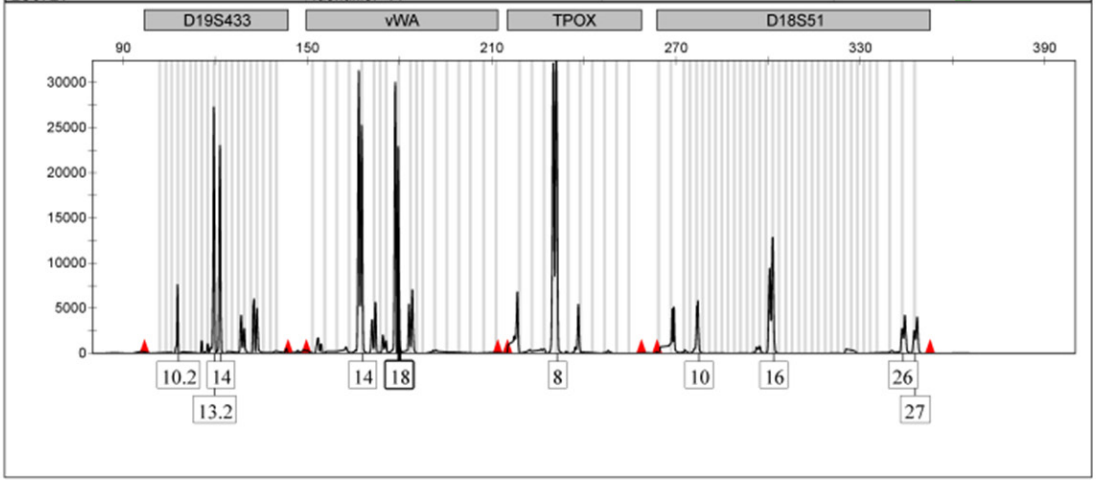

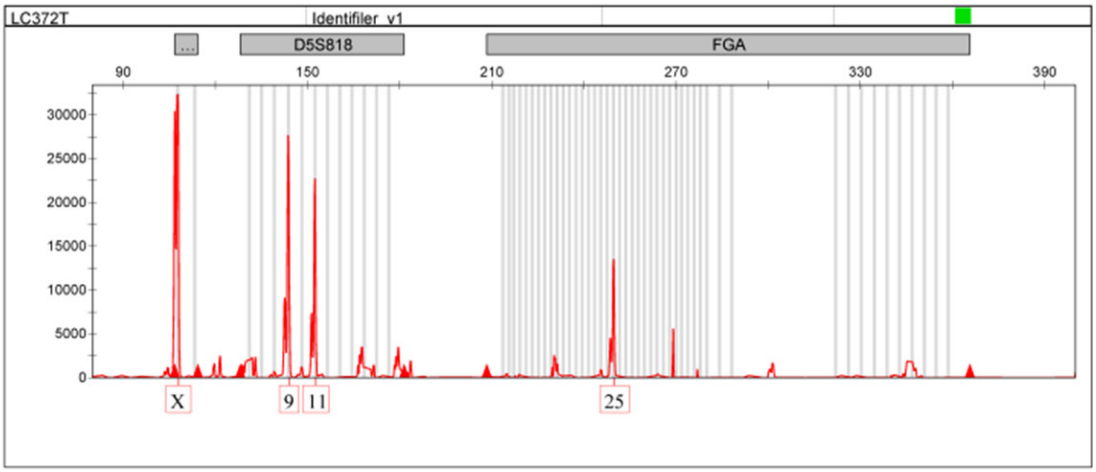

Sun Nov 21,2021 07:39PM, PST Printed by: gm Page 2 of 2

STR analysis for HCC374

■ STR loci genotype ：

Locus Name	D5S818	D13S317	D7S820	D16S539	vWA	TH01	AMEL	TPOX	CSF1PO
Allele genotype	10,11	10,10	11,11	9,11	17,19	6,7	x,x	8,8	12,12

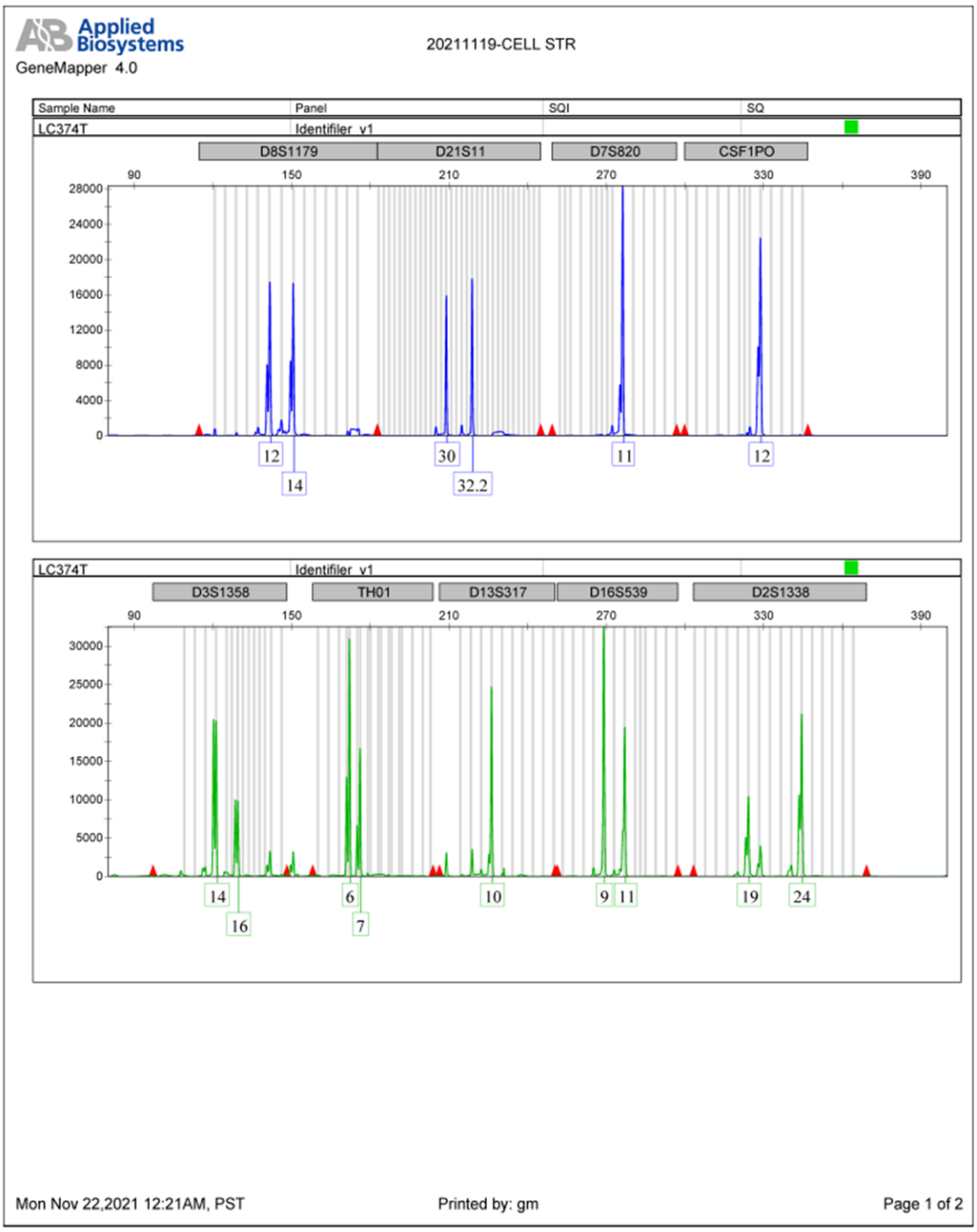

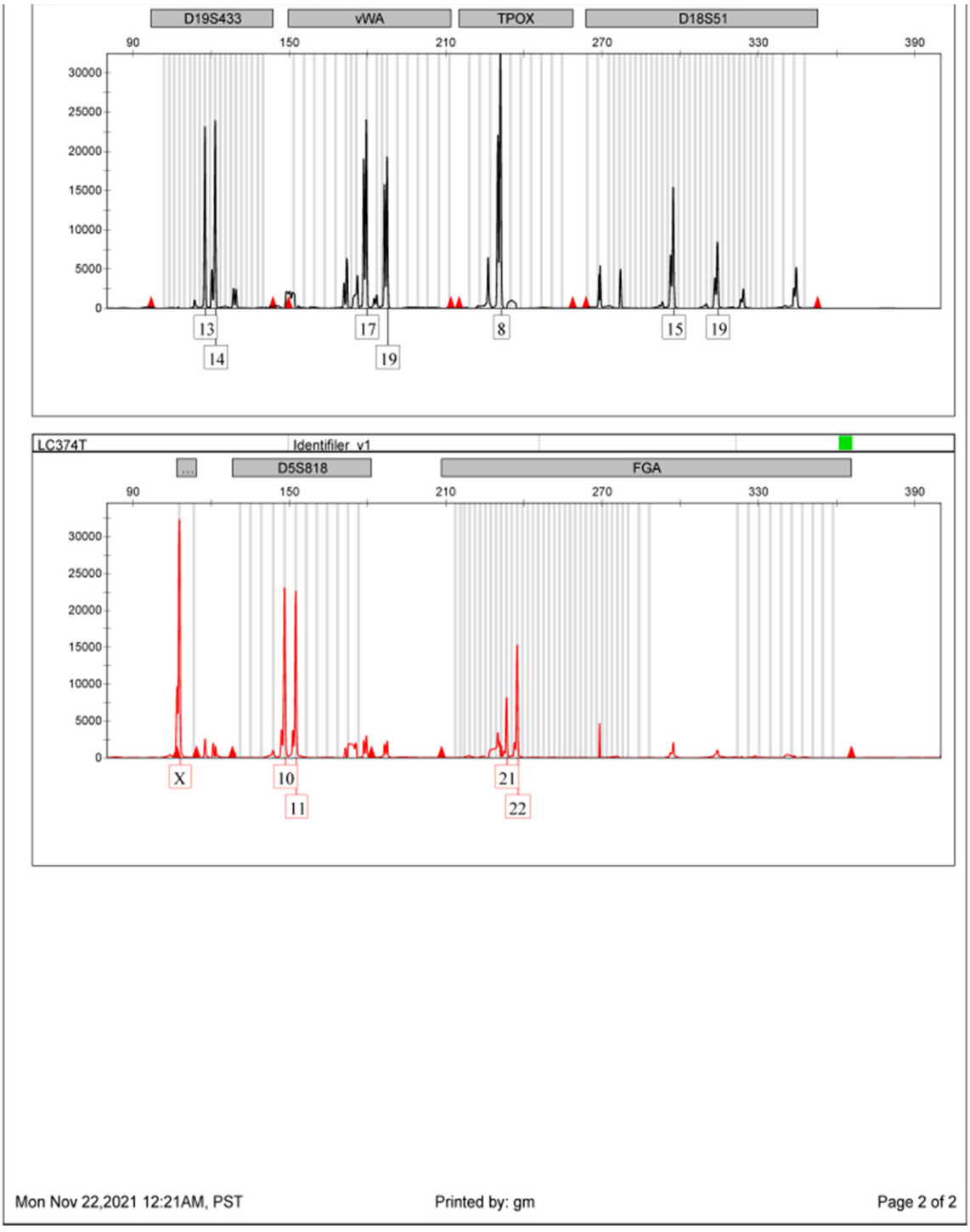

Supplementary Figure 1. Reports for authentication of the patient-derived HCC cell lines: LC372T (HCC372), LCHCC374T (HCC374) by human STR.

Supplementary Table 1. Primers for RT-PCR in gene expression analysis

Gene	Primer sequence	Product size
Snail	F: 5'AAGC TTCC ATGG CGCG CTCT TTCC TCGT CAGG AAGC CC3'	795 bp
	R: 5'GGAT CCTC AGCG GGGA CATC CTGA GCAG CCGG ACTC TTG3'	
FN	F: 5'AAG GAG AAG ACC GGA CCA AT3'	314 bp
	R: 5'GGC TTG ATG GTT CTC TGG AT3'	
GADPH	F: 5'ACC ACA GTC CAT GCC ATC AC3'	452 bp
	R: 5'TCC ACC ACC CTG TTG CTG TA3'	
Hic5	F: 5AGC CCC GCC CCT AAG GTA CTA T3'	251 bp
	R: 5'GTA GGT AGA AAA AGT GCA CAG AAC AGT GAG3'	
ZNF395	F: 5CGA AAA AAG AAA GAA CTC TGT G3'	122 bp
	R: 5'CTG TGT CCC CCC AGA TGG AG3'	
ROMO1	F: 5CTG TCT CGA GAT CGG AAT GCG3'	114 bp
	R: 5'CAT CGG ATG CCC ATC CCA ATG3'	
MMP9	F: TGTACCCTATGTACCGCTTCA	1283 bp
	R: AGAAGAAAAGCTTCTTGGAGA	

Supplementary Table 2. Criteria for evaluating metastatic potentials

Metastatic potential / Metastatic index	+++[a]	++	+	0
Lympho/vascular invasion	√[b]	√	√	-
Perineural invasion	√	-	-	-
Regional lymph nodes involved	M[c] > 10	5 < M < 10	0	0

a: the text of metastatic potential. b: represent the presence of indicated metastatic index. c: M represents the numbers of lymph nodes.

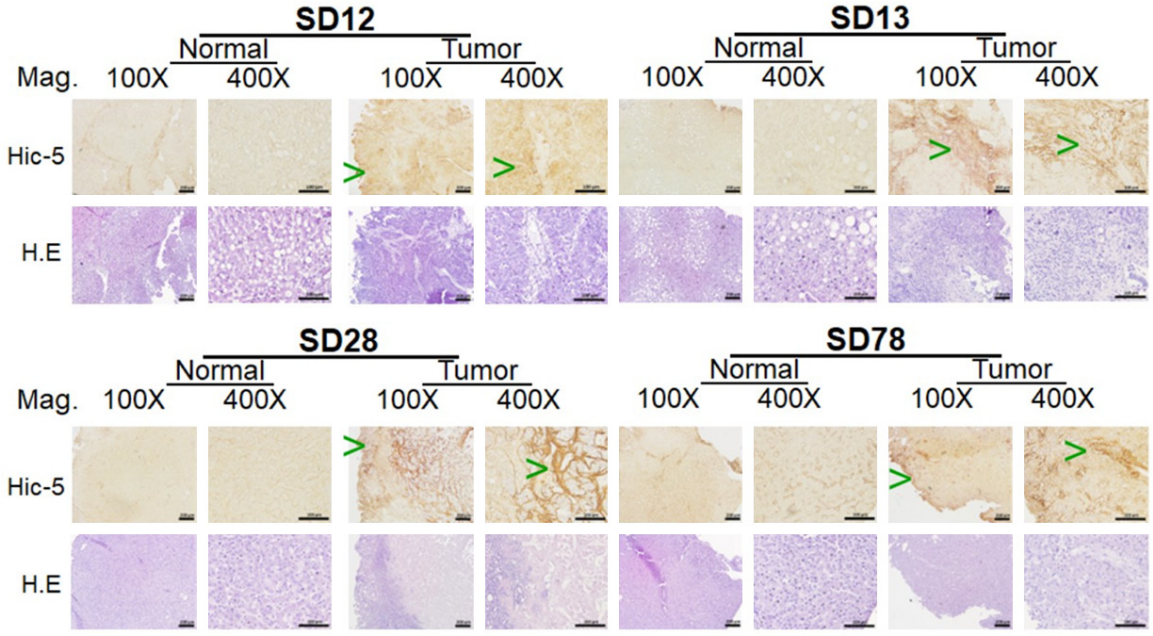

Supplementary Figure 2. IHC of Hic-5 in clinical HCC tissues. IHC of Hic-5 on tumor and normal counterpart of indicated HCCs. H.E. stains for each sample are included. Arrow head indicate the location of high Hic-5 staining region in tumor section under 100- and 400-fold of magnification. The results shown were representatives of two reproducible data.

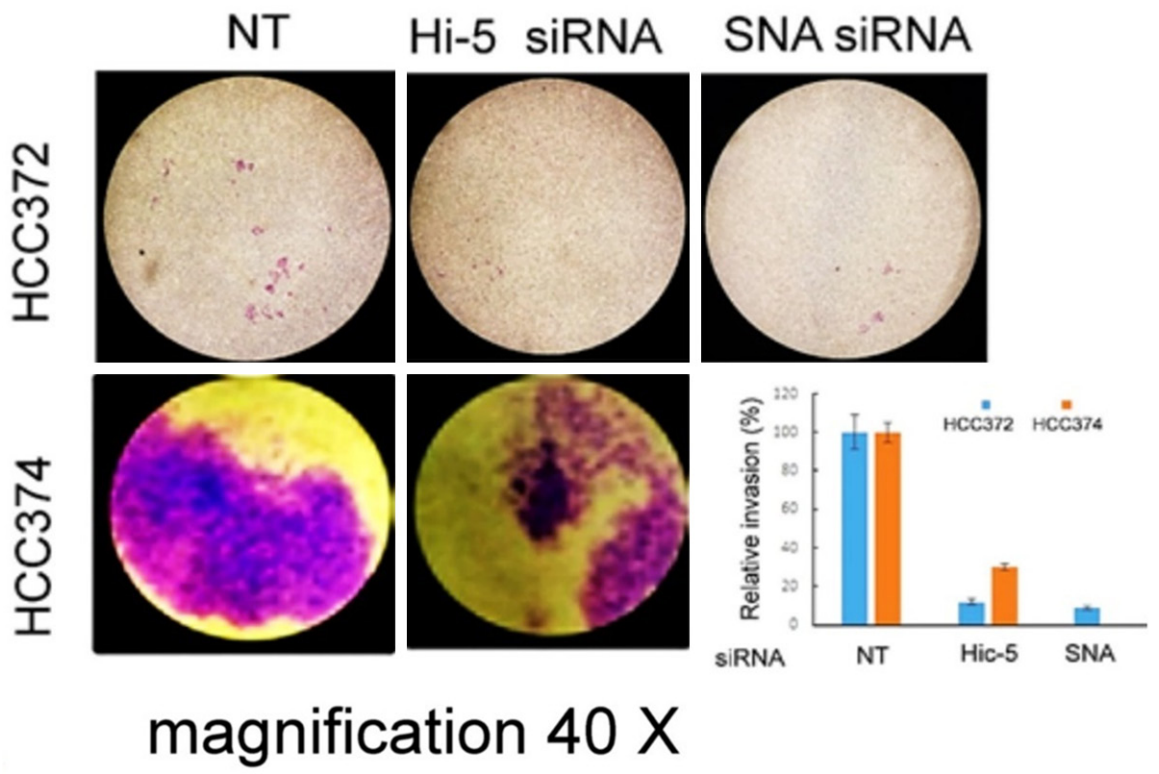

Supplementary Figure 3. Knockdown of Hic-5 and SNA suppressed HCC 372/374 invasion. HCC372 (upper panel) and HCC374 (lower panel) cells were transfected with Hic-5 (at 25 nM) or SNA siRNA at 50 nM for 48 h. Transwell invasion assay was performed. The images of crystal violet-stained invaded HCC cells were pictured under phase contrast microscope at 40× magnification. Nontargeting (N-T) siRNA is the negative control group. Quantitative data for both cells obtained by Image J is shown in the lower right panel. Relative invasion was calculated, taking the results of NT group as 100%. The data shown are average of two reproducible results with C.V. of 8.5%.

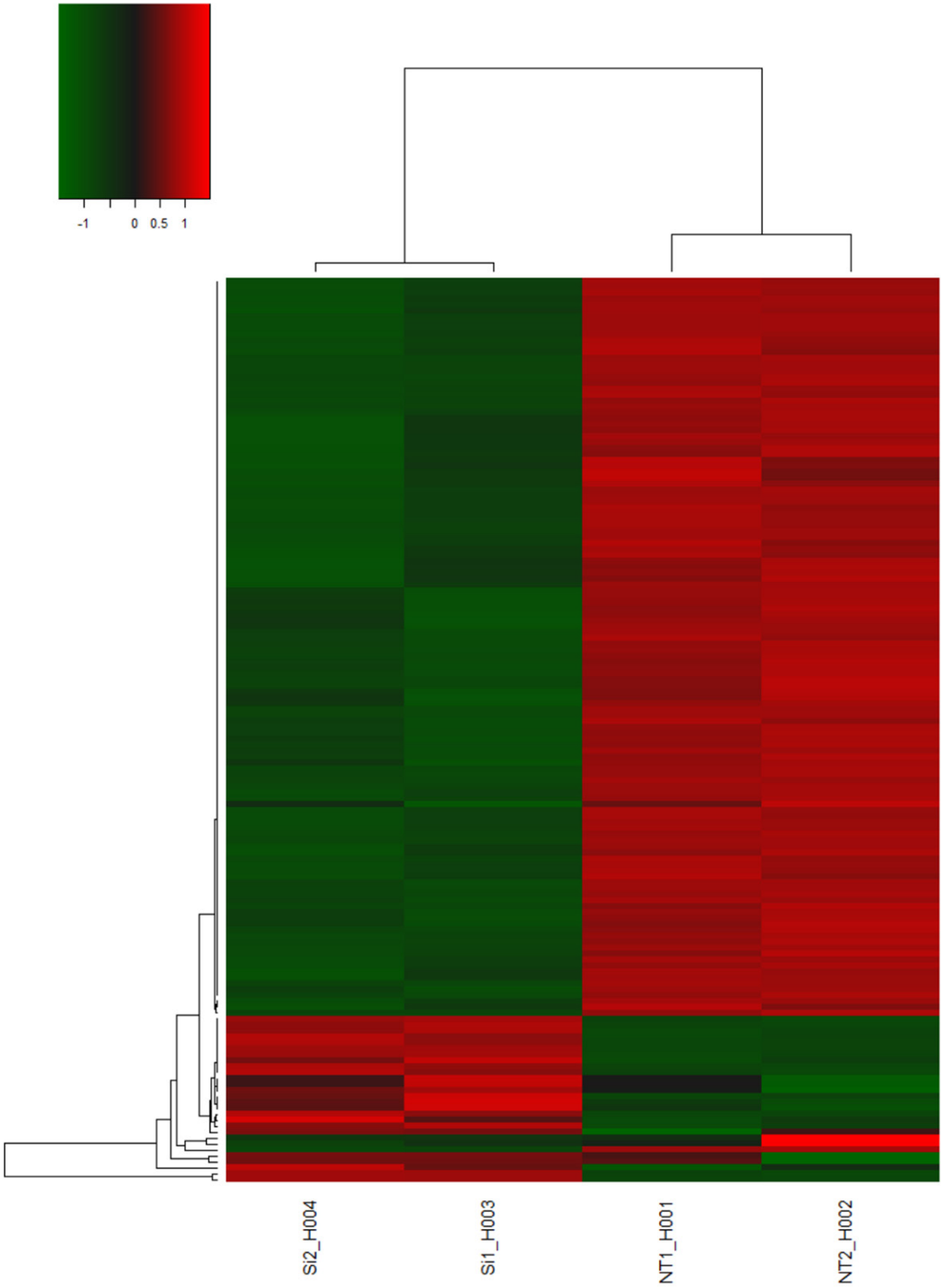

Supplementary Figure 4. Clustering analysis for correlation of expression profiles between Hic-5 siRNA- versus NT siRNA- transfected HCC372. Total mRNA of HCC372 transfected with Hic-5 siRNA (25 nM) or nontargeting RNA were extracted for detecting the amount of gene expressions altered in Hic-5-depleted cells. For advanced data analysis, intensity data were pooled and calculated to identify differentially expressed genes based on the threshold of fold change and *p*-value. The correlation of expression profiles between samples and treatment conditions was demonstrated by unsupervised hierarchical clustering analysis. Clustering was performed to visualize the correlations

among the replicates and varying sample conditions. Up- and down-regulated genes are represented in red and green colors, respectively. A subset of differential genes was selected for clustering analysis. For this microarray project, the number of genes clustered was 152.

Supplementary Table 3. Number of differentially expressed genes for hic-5 siRNA versus NT siRNA

Item	Comparison	Up-regulated	Down-regulated*
1	Si/NT	25	127

*Standard selection criteria to identify differentially expressed genes are as follows: log2|Fold change| ≥ 1 and P < 0.05.

Supplementary Table 4. Identification of 127 Hic-5 upregulated gene by clustering analysis

Phalanx_id	Normalized intensity		Si/NT		Gene_symbol
	Si	NT	logFC	*P*. Value	
PH_hs_0001028	22796.5659	50859.3067	-1.1576953	1.9906E-05	SEC61G
PH_hs_0001371	1920.269	3887.51459	-1.0175397	0.00020932	MRPL33
PH_hs_0002367	2005.94598	4560.06562	-1.1847718	4.0711E-05	TAF5L
PH_hs_0002682	4229.3551	9423.98289	-1.1558992	3.5434E-05	NDUFA8
PH_hs_0002734	4170.86907	9195.69515	-1.1406106	2.7811E-05	ZNF395
PH_hs_0003031	654.655282	1554.93505	-1.248047	1.201E-05	TRIOBP
PH_hs_0003866	847.54424	1745.45738	-1.0422445	4.4744E-05	VWCE
PH_hs_0004116	28213.1357	61531.2946	-1.1249533	2.4212E-05	COX7A2
PH_hs_0004525	3427.83196	8755.23617	-1.3528497	8.3914E-06	JUN
PH_hs_0004800	5431.46867	11385.1913	-1.0677443	3.7078E-05	NDUFC1
PH_hs_0004825	4806.10337	14111.8357	-1.5539661	3.1909E-06	ATP5I
PH_hs_0005071	2075.69362	4385.65177	-1.0791978	3.3008E-05	KHSRP
PH_hs_0005211	194.906721	392.608863	-1.0103089	5.677E-05	SOX15
PH_hs_0007437	1467.50416	3109.12887	-1.0831458	3.0706E-05	LINC00116
PH_hs_0009709	594.643016	1302.34051	-1.131011	3.2295E-05	NA
PH_hs_0010222	1485.65593	3136.67203	-1.0781347	2.9225E-05	SEMA7A
PH_hs_0010373	400.154523	975.06192	-1.2849366	1.6537E-05	NA
PH_hs_0012660	4625.68089	9921.32639	-1.1008673	2.6129E-05	NDUFB4
PH_hs_0012820	4775.97772	10207.1731	-1.0957153	0.00011997	ATP5J2
PH_hs_0013741	289.524216	685.298446	-1.2430484	1.798E-05	APOC1
PH_hs_0014427	3647.97638	7326.69091	-1.0060654	6.5484E-05	ATOX1
PH_hs_0016142	6396.15942	14976.556	-1.2274281	6.4398E-05	SLIRP
PH_hs_0016330	10664.1153	21877.0257	-1.0366523	5.1342E-05	NAA38
PH_hs_0017297	17963.0552	36235.5825	-1.0123743	0.00016199	COMMD6
PH_hs_0019028	1483.77593	2972.26421	-1.0022891	7.1952E-05	NOP14
PH_hs_0019645	8597.24332	17643.4363	-1.0371855	3.7528E-05	S100A11
PH_hs_0019972	6612.55646	14016.7954	-1.0838765	8.0844E-05	COX6B1
PH_hs_0021034	20889.4778	42445.6576	-1.0228405	6.2765E-05	POLR2L
PH_hs_0022069	11128.8084	26225.4775	-1.2366699	1.6853E-05	NDUFB2
PH_hs_0023141	1570.95351	3744.92095	-1.2532948	1.6646E-05	RDH11
PH_hs_0023152	3985.51448	7999.81534	-1.0052007	4.7104E-05	C19orf53
PH_hs_0024397	5404.60569	11346.1711	-1.0699443	6.8526E-05	UBL5
PH_hs_0024614	4759.52452	9716.85312	-1.0296717	6.7238E-05	TAF15
PH_hs_0026695	3755.3531	7797.54809	-1.054072	4.7393E-05	HYPK|SERF2-C15ORF63
PH_hs_0027726	6099.29056	12360.3883	-1.0190107	0.00011091	DYNC1I2
PH_hs_0028878	6809.91274	14697.8292	-1.1098949	3.6065E-05	NDUFA12
PH_hs_0028888	42287.7403	115263.475	-1.446624	8.206E-06	HIST1H4C
PH_hs_0029003	12402.6686	27878.3455	-1.1684944	3.4214E-05	RPL37
PH_hs_0029098	4180.85913	8628.28107	-1.0452737	5.3797E-05	TOMM7
PH_hs_0029324	7512.28094	16067.3126	-1.0968057	7.5757E-05	TCEB2

PH_hs_0029413	461.83593	981.120143	-1.0870494	2.9592E-05	NDUFA3
PH_hs_0029827	19454.1491	46199.5238	-1.2478001	1.3534E-05	COX6C
PH_hs_0030161	33224.1917	70572.6051	-1.0868742	3.1047E-05	COX7B
PH_hs_0030178	23226.598	55663.096	-1.2609433	1.2762E-05	RPS17
PH_hs_0030244	12240.4607	25678.7786	-1.0689187	3.6368E-05	SNRPG
PH_hs_0030426	35034.87	76863.4789	-1.1335067	9.9689E-05	RPL36A
PH_hs_0030896	203.590027	427.948939	-1.0717718	8.8083E-05	TFF2
PH_hs_0030976	398.618369	960.008968	-1.2680397	1.8931E-05	NFKBIB
PH_hs_0030989	4697.90636	9827.85592	-1.0648588	5.0562E-05	RNF181
PH_hs_0031013	27729.0183	58373.1994	-1.0739096	4.4272E-05	MRPL33
PH_hs_0031138	8480.68016	19542.2765	-1.2043467	2.762E-05	NDUFA8
PH_hs_0031203	8187.32864	27024.2301	-1.7227888	9.8476E-07	HIST1H4C
PH_hs_0031518	9241.74779	19285.4382	-1.0612743	0.00010585	C14orf2
PH_hs_0032964	6874.74802	14095.191	-1.0358243	4.0032E-05	SPANXD|SPANXA2|SPANXA1|SPANXB1|SPANXC
PH_hs_0033317	1816.25402	4318.39604	-1.2495296	3.572E-05	TMEM256
PH_hs_0033839	40537.8333	85427.2199	-1.0754269	3.0161E-05	RPL37
PH_hs_0034289	582.273852	1665.33551	-1.5160431	3.168E-06	NA
PH_hs_0034946	4203.34966	8626.22665	-1.0371901	0.00015336	RPL36
PH_hs_0035339	6846.37904	14292.6749	-1.0618629	3.1986E-05	UQCR11
PH_hs_0035365	4745.0245	9641.87313	-1.0228979	7.3065E-05	COX17
PH_hs_0035451	19308.3857	43469.2578	-1.1707679	4.1953E-05	NDUFA1
PH_hs_0035627	3077.76374	6754.43856	-1.1339534	3.6738E-05	NDUFA2
PH_hs_0035828	28828.2704	59638.8633	-1.0487685	0.00111465	GTF2H5
PH_hs_0035956	34289.2684	69035.1886	-1.0095748	4.5086E-05	COX7B
PH_hs_0035962	1504.87949	3692.49421	-1.2949477	9.5123E-06	SMIM4
PH_hs_0036096	17061.3264	38900.0362	-1.1890417	3.1389E-05	USMG5
PH_hs_0036101	11134.4499	23318.5415	-1.0664473	4.2441E-05	OST4
PH_hs_0038203	8041.19742	17764.2145	-1.1434916	0.00014075	SPANXD|SPANXA2|SPANXA1
PH_hs_0038876	30608.5889	74952.7868	-1.2920456	9.8436E-06	MT2A
PH_hs_0040048	8814.46188	20389.4057	-1.2098753	2.0165E-05	MT1E
PH_hs_0042013	50	126.213006	-1.3358606	7.2134E-06	C2CD3
PH_hs_0042014	1377.50473	3297.68035	-1.2593943	3.6447E-05	SMIM4
PH_hs_0042034	85307.228	192636.075	-1.175138	1.6374E-05	RPL37A
PH_hs_0042093	10838.8309	23505.0286	-1.1167603	3.0485E-05	TMEM258
PH_hs_0042150	24213.5605	48584.4314	-1.0046788	0.00017462	COX6C
PH_hs_0042192	2100.86196	4846.36451	-1.2059215	1.4196E-05	C5orf58
PH_hs_0042460	2010.62789	4065.2117	-1.0156844	0.0002848	ADIRF
PH_hs_0042520	201.945671	431.060008	-1.0939215	7.9854E-05	RNASE7
PH_hs_0042526	28779.64	81186.1829	-1.4961857	1.3108E-05	OR4D6
PH_hs_0042874	7318.69113	14758.3836	-1.0118772	0.00024473	CENPW
PH_hs_0043120	1229.9231	2893.52313	-1.2342591	1.1491E-05	IL10RB
PH_hs_0043195	7893.54916	16868.2027	-1.0955602	3.8576E-05	PPDPF
PH_hs_0043217	252.894706	746.440647	-1.5614907	0.04774558	FGD4
PH_hs_0043313	4272.03445	10795.7079	-1.3374627	9.4474E-06	ROMO1
PH_hs_0043344	3810.63267	7897.65982	-1.0513947	6.2643E-05	FBXL17
PH_hs_0043882	41030.5155	118791.027	-1.5336567	4.6798E-06	RPL38
PH_hs_0043889	28539.3193	65855.103	-1.2063443	8.942E-05	USMG5
PH_hs_0044059	15997.5322	36122.8308	-1.1750616	2.241E-05	NA
PH_hs_0044630	1626.99825	3375.46207	-1.0528723	8.137E-05	DPM3
PH_hs_0044870	4253.10762	8511.59812	-1.0009127	0.00024173	CHCHD10
PH_hs_0044898	32329.6792	65904.8909	-1.0275263	4.7542E-05	COX6A1
PH_hs_0045557	17609.9868	37391.8342	-1.0863294	0.00011727	RPL36
PH_hs_0045560	32325.3562	85836.7758	-1.4089296	5.9329E-05	RPS29

PH_hs_0045784	967.303699	2095.00804	-1.114915	2.7778E-05	MT1A
PH_hs_0046059	2193.45085	5031.65139	-1.1978296	3.1638E-05	MED18
PH_hs_0046273	5414.90059	13057.1851	-1.2698372	3.4266E-05	MYEOV2
PH_hs_0047500	8143.73906	16510.9984	-1.0196641	5.7189E-05	CTSB
PH_hs_0047576	3159.3025	6359.18929	-1.0092368	0.00015683	GXYLT1
PH_hs_0047675	72.3577945	397.565105	-2.4579708	0.01997172	RAPGEF5
PH_hs_0048688	2581.63717	6333.32744	-1.2946774	1.4283E-05	U2AF2
PH_hs_0048795	3768.38689	8150.59518	-1.1129583	4.6382E-05	HAUS2
PH_hs_0049199	7175.43963	15791.2658	-1.1379877	9.6267E-05	DDX6
PH_hs_0049222	4273.4266	8559.32767	-1.0021041	0.00013135	CDK6
PH_hs_0049243	566.12093	1409.64549	-1.3161502	7.0189E-06	ANKRD52
PH_hs_0049488	18188.3797	39022.5627	-1.1012915	9.2468E-05	ATP5E|SLMO2-ATP5E|ATP5EP2
PH_hs_0049578	21681.3862	46017.4746	-1.0857248	0.00017007	SNRPG
PH_hs_0049631	473.179024	1411.00201	-1.576262	4.419E-06	MT1IP|MT1X|MT1E|MT1A|MT2A|MT1B|MT1L|MT1H
PH_hs_0060018	44009.6839	93378.5347	-1.0852699	3.9405E-05	TMA7
PH_hs_0060515	83483.1559	175499.535	-1.0719102	4.3422E-05	RPS29
PH_hs_0061007	53.0028062	469.68358	-3.1475485	1.4649E-08	NA
PH_hs_0061465	31185.194	64767.5284	-1.0544095	6.6821E-05	ROMO1
PH_hs_0061501	3647.70424	7332.77289	-1.0073701	0.00016582	NAA38
PH_hs_0061630	16551.1035	36488.1091	-1.140499	2.4833E-05	ACTN4
PH_hs_0061953	1988.69153	4842.59026	-1.2839594	8.1038E-06	C4orf48
PH_hs_0061957	2461.76719	6261.50822	-1.3468159	1.626E-05	PET100
PH_hs_0062243	20831.8767	52771.1412	-1.3409564	1.0639E-05	SPANXC|SPANXA2|SPANXA1|SPANXB1|SPANXD
PH_hs_0062253	12912.5947	27506.9014	-1.0910147	0.00010732	SPANXB1|SPANXC|SPANXD|SPANXA2|SPANXA1
PH_hs_0062274	2701.92948	5545.01117	-1.0372003	0.00011354	BAGE2|BAGE4|BAGE3|BAGE5
PH_hs_0062302	12605.5533	30714.3396	-1.2848529	8.3053E-06	PAGE2|PAGE2B|PAGE5
PH_hs_0062772	408.93569	916.815268	-1.1647571	2.5228E-05	MT1F
PH_hs_0062793	195.615681	511.188729	-1.385834	4.9472E-05	MT1G
PH_hs_0062856	58226.4575	116992.576	-1.0066702	6.8365E-05	RPS26|RPS26P11|LOC101929876|LOC100996747
PH_hs_0062866	46415.088	103399.106	-1.155558	5.6867E-05	RPS26|RPS26P11|LOC101929876|LOC100996747
PH_hs_0063085	140.511826	300.574209	-1.0970297	4.1685E-05	NA
PH_hs_0063186	2343.81954	5221.75941	-1.1556745	2.587E-05	NA
PH_hs_0063254	3122.22514	7847.20147	-1.3296037	1.2681E-05	NA
PH_hs_0063621	65677.9786	155010.409	-1.2388835	2.4201E-05	RPS28

The signal intensities of 127 genes which were lower in Hic-5siRNA transfected HCC372 than those of nontargeting (N-T) siRNA group are demonstrated in second column. Third column shows the ratio of logFC for Hic-5siRNA vs that of N-T siRNA group. The id of the genes under analysis and their gene symbol are shown in first and fourth columns, respectively. Two of the metastasis related genes ZNF395 and ROMO are marked in red.

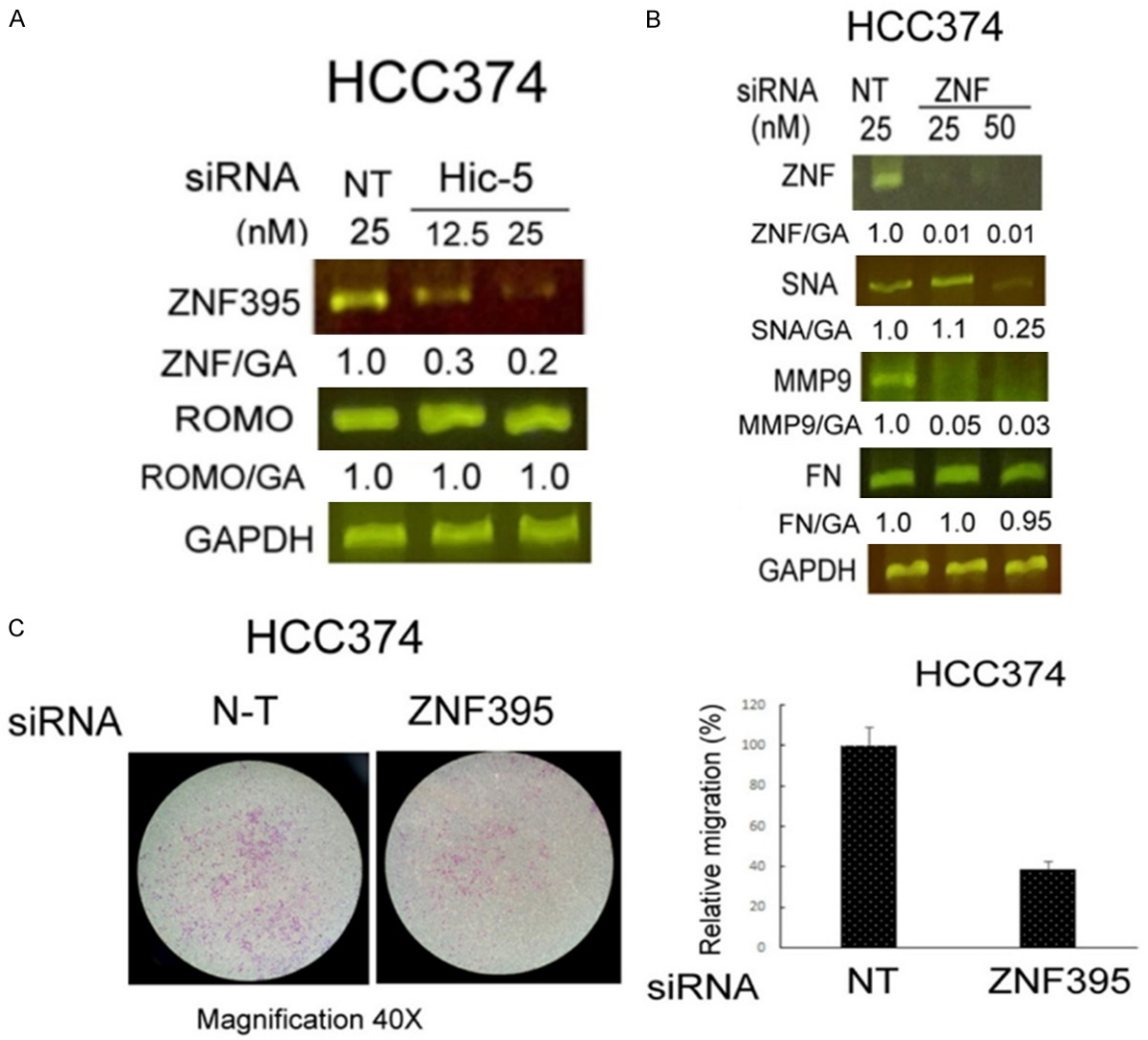

Supplementary Figure 5. ZNF395 but not ROMO is upregulated by Hic-5 mediated pathway required for the expression of mesenchymal genes and migration in HCC374. HCC374 cells were transfected with siRNA against Hic-5 (A) and ZNF395 (B), and (C) at indicated concentrations (nM). RT-PCR (A, B) and cell migration assay (C) were performed. N-T siRNA is the negative control group. In (A) and (B), GAPDH is an internal control. The numbers below each band denote the relative intensities (averages of data from three reproducible experiments) for indicated molecules versus GAPDH (coefficient of variation [C.V.]: 5%), using the data of the N-T group as 1.0. In (C), images of crystal violet-stained migrated HCC cells were captured under a phase contrast microscope at 40-fold magnification and quantified using the Image J software. Relative motility was calculated, using the data of the N-T group as 100% (right panel). * indicated the statistical significance ($P < 0.05$) between the indicated samples *vs* the N-T group (n = 3).